

TELECENTRIC ZOOM LENSES

by

Ross T Terrill

Copyright © Ross T Terrill 2020

A Thesis Submitted to the Faculty of the
JAMES C. WYANT COLLEGE OF OPTICAL SCIENCES

In Partial Fulfillment of Requirements

For the Degree of

MASTER OF SCIENCE

In the Graduate College

THE UNIVERSITY OF ARIZONA

2020

THE UNIVERSITY OF ARIZONA
GRADUATE COLLEGE

As members of the Master’s Committee, we certify that we have read the thesis prepared by **Ross T. Terrill**, titled *Telecentric Zoom Lens* and recommend that it be accepted as fulfilling the thesis requirement for the Master’s Degree.

 <hr/> Professor José M. Sasián	Date: <u>11/23/20</u>
 <hr/> Professor Daewook Kim	Date: <u>11/23/2020</u>
 <hr/> Professor Yuzuru Takashima	Date: <u>11/23/2020</u>

Final approval and acceptance of this thesis is contingent upon the candidate’s submission of the final copies of the thesis to the Graduate College.

I hereby certify that I have read this thesis prepared under my direction and recommend that it be accepted as fulfilling the Master’s requirement.


 <hr/> Professor José M. Sasián Master’s Thesis Committee Chair Wyant College of Optical Sciences	Date: <u>12/01/2020</u>
---	-------------------------



Table of Contents

List of Figures	4
List of Tables	7
Abstract	8
1 Introduction.....	10
2 First-Order Analysis.....	15
2.1 Telecentric First-Order Analysis.....	19
2.2 Multi-configuration Telecentric First-Order Analysis	21
3 Third-Order Analysis	26
3.1 Spherical Aberration	29
3.2 Coma	31
3.3 Astigmatism	33
3.4 Field Curvature.....	34
3.5 Distortion.....	35
3.6 Chromatic Aberrations	37
3.7 Pupil Aberrations.....	39
4 Third-Order Zoom Lens Design	43
4.1 Study 1.....	44
4.2 Study 2.....	51
5 Results and Discussion	58
Appendix A - Glossary	65
Appendix B - Software Source Code.....	69
References.....	71

List of Figures

Figure 1: Illustration of the anatomy of a First Order system with key components indicated.	12
Figure 2: Illustration of vignetting in an optical system resulting in the off-axis rays being clipped by the aperture of the lens.	13
Figure 3: Illustration of divergence between θ and $\sin\theta$ from 0° to 90°	17
Figure 4: Illustration of divergence between first, third, and fifth order Taylor series expansion for $\sin\theta$ from 0° to 90°	17
Figure 5: Illustration of percentage error between first, third, and fifth order Taylor series expansion for $\sin\theta$ from 0° to 90°	18
Figure 6: First-order model of an Image-Space Telecentric system.....	19
Figure 7: First-order model of an Double-Sided Telecentric system	19
Figure 8: First-order model of a zoom a N-P Image-Space Telecentric zoom system with 40° field of view, with an effective focal length of 200 (top), 325 (middle), and 500 mm(bottom).....	22
Figure 9: First-order model of a zoom a P-N Image-Space Telecentric zoom system with 40° field of view, with an effective focal length of 200 (top), 325 (middle), and 500 mm(bottom).....	23
Figure 10: First-order model of a zoom a N-P Object-Space Telecentric zoom system with 40° field of view, with an effective focal length of 200 (top), 325 (middle), and 500 mm(bottom).....	24
Figure 11: First-order model of a multi-configuration Telecentric system based on an existing zoom system. F/6, F/8, F/10, 10° Field of View, with an effective focal length of 25 (top), 50 (middle), and 75 mm(bottom).....	25
Figure 12: Illustration of optical system with the field vector, H , scaled by the chief ray height, y_0 , at the object plane, and the aperture vector, ρ , scaled by the marginal ray height, $y' E$, at the exit pupil. A first-order ray shown as a dotted line, and the real ray shown as a solid line.	26
Figure 13: Example of a ray caustic resulting from Spherical Aberration.	29
Figure 14: Visualization of the waveform deformation resulting from Spherical Aberration.....	30
Figure 15: Transverse ray plot of Spherical Aberration.	30
Figure 16: Example of a ray caustic resulting from Coma Aberration.....	31
Figure 17: Visualization of the waveform deformation resulting from Coma Aberration.	31
Figure 18: Transverse ray plot of Coma Aberration.....	32
Figure 19: Visualization of the waveform deformation resulting from Astigmatism.....	33
Figure 20: Transverse ray plot of Astigmatism.	33
Figure 21: Visualization of the waveform deformation resulting from Field curvature.....	34
Figure 22: Transverse ray plot of Field curvature.	34
Figure 23: Visualization of the waveform deformation resulting from Distortion.....	35
Figure 24: Transverse ray plot of Distortion.	35
Figure 25: Dispersion Diagram for the index of refraction of N-BK7 glass against wavelength in the visible spectrum.	37
Figure 26: A glass map of different catalogs of manufacturers' glass plot with Index of Refraction against Abbe Number	38
Figure 27: Illustration of the wondering pupil and the difference between the First Order Chief Ray compared to Real Chief Ray resulting from the aberrations present in the system.....	42
Figure 28: Multi-configuration zoom lens. F/5, F/6.2, F/7.8, 11.6° Field of View, with an effective focal length of 25 (top), 50 (middle), and 75 mm (bottom).....	44
Figure 29: Tangential and Sagittal ray fan of sample zoom lens, with a field of 0.0° at a focal length of 25, 50, and 75 mm, from left to right, using a scale of $\pm 100.0 \mu\text{m}$	46
Figure 30: Tangential and Sagittal ray fan of sample zoom lens, with a field of 4.1° at a focal length of 25, 50, and 75 mm, from left to right, using a scale of $\pm 100.0 \mu\text{m}$	46
Figure 31: Tangential and Sagittal ray fan of sample zoom lens, with a field of 5.8° at a focal length of 25, 50, and 75 mm, from left to right, using a scale of $\pm 100.0 \mu\text{m}$	46

Figure 32: Field curvature and distortion plots of sample zoom lens, at a focal length of 25, 50, and 75 mm from left to right, using a scale of ± 2.0 mm and ± 1.0 %	46
Figure 33: Multi-configuration zoom lens which maintains telecentricity. F/5, F/6, F/8, 4° Field of View, with an effective focal length of 25 (top), 50 (middle), and 75 mm (bottom) with the stop positioned to maintain telecentricity.	47
Figure 34: Tangential and Sagittal ray fan of Study 1, with a field of 0.0° at a focal length of 25, 50, and 75 mm, from left to right, using a scale of ± 100.0 μm	49
Figure 35: Tangential and Sagittal ray fan of Study 1, with a field of 1.4° at a focal length of 25, 50, and 75 mm from left to right, using a scale of ± 100.0 μm	49
Figure 36: Tangential and Sagittal ray fan of Study 1, with a field of 2.0° at a focal length of 25, 50, and 75 mm from left to right, using a scale of ± 100.0 μm	49
Figure 37: Field curvature and distortion plots of Study 1, at a focal length of 25, 50, and 75 mm from left to right, using a scale of ± 2.0 mm and ± 1.0 %	49
Figure 38: Visualization of the degree of telecentricity of the telecentric zoom lens expressed as a percentage across a normalized pupil.	50
Figure 39: Multi-configuration zoom lens. F/4.6, 12.0° Field of View, with an effective focal length of 62 (top), 82 (middle), and 168 mm (bottom).	51
Figure 40: Tangential and Sagittal ray fan of <i>US Patent 5,126,833</i> , with a field of 0.0° at a focal length of 62, 82, and 168 mm, from left to right, using a scale of ± 200.0 μm	53
Figure 41: Tangential and Sagittal ray fan of <i>US Patent 5,126,833</i> , with a field of 3.0° at a focal length of 62, 82, and 168 mm, from left to right, using a scale of ± 200.0 μm	53
Figure 42: Tangential and Sagittal ray fan of <i>US Patent 5,126,833</i> , with a field of 6.0° at a focal length of 62, 82, and 168 mm, from left to right, using a scale of ± 200.0 μm	53
Figure 43: Field curvature and distortion plots of <i>US Patent 5,126,833</i> , at a focal length of 62, 82, and 168 mm from left to right, using a scale of ± 0.50 mm and ± 1.0 %	53
Figure 44: Zoom lens described in United States Patent 5,126,883. F7.9, 4° Field of View, with an effective focal length of 62 (top), 82 (middle), and 168 mm (bottom) with the stop positioned to maintain telecentricity.	54
Figure 45: Tangential and Sagittal ray fan of Study 2, with a field of 1.4° at a focal length of 62, 82, and 168 mm, from left to right, using a scale of ± 200.0 μm	56
Figure 46: Tangential and Sagittal ray fan of Study 2, with a field of 1.4 ° at a focal length of 62, 82, and 168 mm, from left to right, using a scale of ± 200.0 μm	56
Figure 47: Tangential and Sagittal ray fan of Study 2, with a field of 2.0° at a focal length of 62, 82, and 168 mm, from left to right, using a scale of ± 200.0 μm	56
Figure 48: Field curvature and distortion plots of Study 2, at a focal length of 62, 82, and 168 mm from left to right, using a scale of ± 0.50 mm and ± 1.0 %	56
Figure 49: Visualization of the degree of telecentricity of the Study 2 expressed as a percentage change of the chief ray angle across a normalized pupil.	57
Figure 50: Through focus spot diagram of Study 1 at configuration 1 with field angle 0.0° (top), 1.4° (middle), and 2.0° (bottom) and the spot size at -100 μm through +100 μm (left to right) with a scale of 400 μm	59
Figure 51: Through focus spot diagram of Study 1 at configuration 2 with field angle 0.0° (top), 1.4° (middle), and 2.0° (bottom) and the spot size at -100 μm through +100 μm (left to right) with a scale of 400 μm	59
Figure 52: Through focus spot diagram of Study 1 at configuration 3 with field angle 0.0° (top), 1.4° (middle), and 2.0° (bottom) and the spot size at -100 μm through +100 μm (left to right) with a scale of 400 μm	60
Figure 53: Through focus spot diagram of Study 2 at configuration 1 with field angle 0.0° (top), 1.4° (middle), and 2.0° (bottom) and the spot size at -100 μm through +100 μm (left to right) with a scale of 400 μm	61
Figure 54: Through focus spot diagram of Study 2 at configuration 2 with field angle 0.0° (top), 1.4° (middle), and 2.0° (bottom) and the spot size at -100 μm through +100 μm (left to right) with a scale of 400 μm	61
Figure 55: Through focus spot diagram of Study 2 at configuration 3 with field angle 0.0° (top), 1.4° (middle), and 2.0° (bottom) and the spot size at -100 μm through +100 μm (left to right) with a scale of 400 μm	62
Figure 56: Grid Distortion plot of Study 1 at Configuration 1 (left), 2 (middle), and 3 (right) shown with an exaggerated 10x scale to clearly show distortion.	63

Figure 57: Grid Distortion plot of Study 2 at Configuration 1 (left), 2 (middle), and 3 (right) shown with an exaggerated 10x scale to clearly show distortion.63

List of Tables

Table 1: Prescription for a sample zoom lens. F/5, F/6.2, F/7.8, 11.6° Field of View, and an effective focal length of 25, 50, and 75 mm.	45
Table 2: Addendum to the prescription for the sample zoom lens showing the multi-configuration distances between lens groups.	45
Table 3: Prescription for Study 1 which maintains telecentricity. F/5, F/6, F/8, 4° Field of View, and an effective focal length of 25, 50, and 75 mm.	48
Table 4: Addendum to the prescription for Study 1 showing the multi-configuration distances between lens groups.	48
Table 5: Seidel Coefficients for Study 1 showing the impact of each aberration on the system, at a focal length of 25, 50, and 75 mm from top to bottom, expressed in waves.	49
Table 6: Prescription for <i>US Patent 5,126,833</i> , which maintains telecentricity. F/4.6, 12° Field of View, and an effective focal length of 62, 82, and 168 mm.	52
Table 7: Addendum to the prescription for <i>US Patent 5,126,833</i> , showing the multi-configuration distances between lens groups.	52
Table 8: Prescription for Study 2 which maintains telecentricity. F7.9, 4° Field of View, and an effective focal length of 62, 82, and 168 mm.	55
Table 9: Addendum to the prescription for Study 2 showing the multi-configuration distances between lens groups.	55
Table 10: Seidel Coefficients for Study 2 showing the impact of each aberration on the system, at a focal length of 62, 82, and 168 mm from top to bottom, expressed in waves.	56

Abstract

The purpose of this thesis is to study multi-configuration imaging systems and to investigate the limitations of maintaining telecentricity across the zoom range. Telecentricity is a property of an optical system which maintains the centroid and height of objects relative to the image plane regardless of axial changes in the position of the object or image. Telecentric zoom lenses provide a unique design challenge with the necessity for telecentric systems to have very low distortion, while distortion is often the dominant residual aberration in a zoom system¹. Additionally, the asymmetric stop position will complicate the correction of other odd aberrations and controlling vignetting in a system with a large usable field of view. This analysis will evaluate the impact of multiple configurations on image-side, object-side, and double-sided telecentric systems² through modeling and simulation. Design considerations and methods are proposed based on an analysis of applications of telecentric zoom lenses, methods for aberration control, and systems which are currently available.

In particular this thesis examines the constraints of designing telecentric systems which can accommodate multiple configurations. Initially idealized first-order telecentric systems are modeled with finite configurations which allow for a zoom ratio of 3, focal length of 25 to 75 mm, and a field of view of 10°. These ideal models are developed with the goal of identifying and minimizing aberrations which will be present in a third-order simulation. A method for describing the degree of telecentricity of a third-order optical system was formed as a function of the aberrations present in the system:

$$\Delta\bar{u} = 4 \cdot \frac{\bar{W}_{040}}{n'\bar{y}_I} - \frac{W_{311}}{n'y_E}$$

Finally, existing designs of third-order multi-configuration systems are modified to provide telecentric performance throughout the zoom range. A zoom ratio of 3, focal length of 25

¹ Chang, Matthew, "Pupil aberration in modular zoom lens design," Ph.D. dissertation, College of Optical Sciences, University of Arizona, AZ, USA, 1998 [Online].

² Miks, Novak, "Design of a double-sided telecentric zoom lens," Department of Physics, Czech Technical University, Prague, Czech Republic, 2012 [Online].

to 75 mm, and a field of view of 4° with a maximum telecentricity of 0.2 %. A second iteration, also with a zoom ratio of 3, a focal length of 62 to 168 mm, and a field of view of 4° with a maximum telecentricity of -0.14 %.

1 Introduction

In photography, a zoom lens is a multi-configuration system which provides the user with an adaptable tool to accommodate many different environments. Typically these systems will be characterized by having a linear movement from a short focal length, known as the wide angle, to a long focal length, known as the telephoto, and maintaining focus throughout the zoomable range. The perspective of spatial distance between objects will seem *flat* at the telephoto configuration compared to the exaggerated spatial distance at the wide angle configuration. For applications where spatial depth is unwanted, an extreme telephoto lens, or telecentric lens, can be used to remove perspective from the imaging system. Telecentric lenses are characterized by having large useable depth of field or depth of focus, exceptionally low distortion, and low paraxial error across the field of view³.

Telecentric lenses are compound optical systems which maintain the centroid and height of objects relative to the image plane, regardless of the object position with respect to a given nominal image plane position, the focus will take place. Telecentricity is achieved by maintaining the location of the entrance pupil, the exit pupil, or both at infinity, and are commonly referred to as *object-space*, *image-space*, and *double-sided telecentric*, respectively. The pupil will be located at infinity by placing the aperture stop at the focal plane of the system, the front focal plane for *image-space telecentric* and the rear focal plane for *object-space telecentric*.

Depth of field is a concept related to object space and defines the displacement of an object along the optical axis, while the image quality is maintained. A related concept is depth of focus which defines the displacement in image space along the optical axis, and image quality is maintained. Object-space telecentric lenses can accommodate a shift in object space, whereas image-space telecentric lenses can accommodate a shift in image space while maintaining focus. The criteria for image quality is determined by the application and is commonly the smallest detectable blur, e.g. a pixel size.

³ Hu,Haosheng “Tutorial of Telecentric Lens”, Tutorial , College of Optical Sciences, University of Arizona, AZ, USA, 2016 [Online].

Low distortion is also a characteristic of telecentric systems, where distortion aberration is a radial deviation from the rectilinear projection and depends on the cube of the field of view. Distortion is defined as *barrel*, *pincushion*, and *mustache*, describing the aberration as positive, negative, or a combination of both. In a distorted system, the image of the object will be skewed near the edge of the field of view, a telecentric system will maintain the ratio of object distances to the ratio of image distances. This allows for accurate and repeatable performance throughout the field of view, regardless of the position of the object.

The orthogonality between the object and the image plane requires that the chief rays remain parallel to the optical axis, this allows for a large amount of information to be imaged through a telecentric system. Imaging sharp contrast changes of an object, such as an edge, as it moves out of focus will result in an asymmetric blur, with a telecentric lens the contrast will remain sharp and provide more vivid results for edge-detection in an image processing analysis.

The focal length of an optical system is a primary descriptive attribute used for either single lenses (singlet) or entire optical systems. The focal length of a system is a metric used to describe the distance from the principal plane to the focal point. The focal length is given by:

$$\frac{1}{f} = \frac{1}{s'} + \frac{1}{s}$$

where, f is the focal length of the system, s is the object distance and s' is the image distance from the respective principal planes. Geometrically, this focal length description can help understand the lateral magnification, m , of a system as the ratio between the height of the image, h' , and the height of the object, h , and can be shown to also relate the object and image distances as:

$$m = \frac{h'}{h} = \frac{s'}{s}$$

The slope, u , of any rays being traced through an optical system is equated through these values as the ratio of the distance by the height:

$$u = -\frac{y}{s}$$

where the ray height is designated as y from h to denote specifically a ray height rather than a generic object height.

The two rays that are most crucial for understanding the performance of an optical system in a ray tracing procedure are the *marginal ray* and the *chief ray*. The *marginal ray* passes through the edge of the aperture stop and through the center of the image, and the *chief ray* passes through the center of the aperture stop and the edge of the image. The *marginal ray* is important for defining the requirements for the diameter of the aperture stop, and the *chief ray* defines the size of the image. With these two rays, the *optical throughput* or capacity of the optical system can be defined⁴. Conventionally u is used to denote the *marginal ray* slope and \bar{u} for the *chief ray* slope. A telecentric system requires that the chief ray is maintained parallel to the optical axis, or:

$$\bar{u} = -\frac{\bar{y}}{\bar{s}} = 0$$

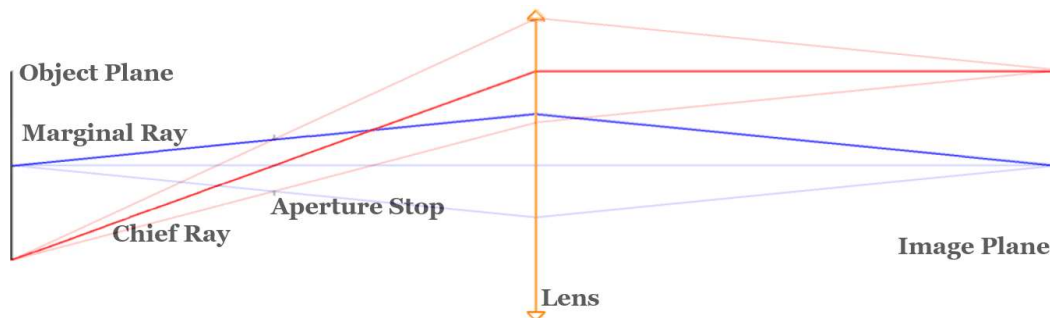


Figure 1: Illustration of the anatomy of a First Order system with key components indicated.

A second descriptive attribute for optical systems is the *f-number* which describes the *speed* or relative aperture of a system and is the ratio of the focal length and the aperture diameter.

⁴ Smith, Warren J. *Modern Optical Engineering Fourth Edition* (New York, NY, McGraw-Hill 2008)

$$f/\# = \frac{f}{D} \approx \frac{n}{2NA}$$

Where NA is the *numerical aperture* of the system which is the product of the index of refraction and the sine of the half angle of the illumination cone.

$$NA = n' \sin U'$$

However, for an object-space telecentric system the entrance pupil is located at infinity and with infinite diameter so the $f/\#$ of the system is not defined⁵.

A larger aperture stop provides a faster imaging system, however the diameter of the stop is limited by a condition called *vignetting*. Vignetting is an obstruction of off-axis rays, which are clipped by the aperture of a lens resulting in a reduction in illumination at the periphery of the field of view. To maintain a uniform transmittance across the exit pupil, the stop diameter will define the field of view which can remain unclipped at the image plane.

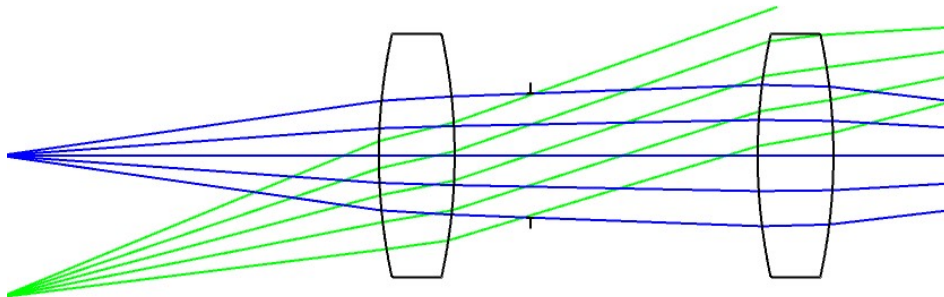


Figure 2: Illustration of vignetting in an optical system resulting in the off-axis rays being clipped by the aperture of the lens.

The third descriptive attribute for optical systems that will be discussed is the *field of view* which describes the portion of the object that is included in the image. This attribute can refer to the *real field of view* describing the region in object space or the *apparent field of view* describing the corresponding region in image space.

Applications for telecentric imaging systems in machine vision and inspection depend on measurements which are made with precise characterization of the optical system

⁵ Hu, Haosheng “Tutorial of Telecentric Lens” College of Optical Sciences, University of Arizona, 2016 [Online]

to ensure that the objects being analyzed are consistently observed. For non-telecentric imaging, a change to the position of the object or imaging system will influence the way that the object being analyzed is perceived. Controlling these tolerances in the field where there is object variation, vibration, system adjustments, and other types of positioning noise will prove to be difficult. Telecentric systems can be used in these applications and provide a more noise invariant solution by allowing for the object to move throughout the field of view or depth of view without resulting in the perspective of the image being changed.

Another application where telecentric lenses are used are microlithographic lenses. Microlithographic lenses are high NA lenses used to transfer large amounts of information between planes. As the information density increases, the impact of aberrations on the system performance also increases. Microlithographic lenses are used in manufacturing integrated circuits (IC) to image a pattern from a photomask to a photosensitive chemical photoresist on the IC wafer substrate. As the density of transistors in ICs have increased, doubling every 18 months in a trend known as Moore's law, the demand for higher performance optics has increased at a similar rate. Although these lenses were wafer side telecentric originally, demand pushed for double sided telecentric lens, and now require multi-configurations to accommodate for aberrations resulting from environmental changes⁶.

⁶ Tomoyuki Matsuyama, Yasuhiro Ohmura, and David M. Williamson "The lithographic lens: its history and evolution", Proc. SPIE 6154, Optical Microlithography XIX, 615403, 2006 [Online].

2 First-Order Analysis

To describe an idealized optical system, a first-order approximation is used to simplify the complexity of the system. A first-order approximation can model an optical system using thin lenses which assumes zero axial thickness of a lens, and allows the principal plane and thin lens to be coincident, it will also adopt the small angle approximation for rays near the optical axis. A thin lens only requires a defined focal length to allow a designer to evaluate the performance and interaction between lenses.

Similar to focal length, optical power is a description of either a singlet or an optical system containing multiple elements, to show the relationship between index of refraction, surface curvature and thickness to the focal length. To understand what influences the power of a system, a general equation for the focal length of a singlet and is given by:

$$\phi = \frac{1}{f} = \frac{(n - n_0)}{n_0} \cdot \left(\frac{1}{R_1} - \frac{1}{R_2} + \frac{(n - n_0)t}{nR_1R_2} \right)$$

where ϕ is the power of the lens, f is the focal length, n is the index of refraction of the lens material, n_0 is the index of refraction of the medium the lens is submerged within, R_1 and R_2 are the radii of curvature of the two surfaces of the singlet, and t is the thickness of the lens along the optical axis. This expression is known as the *lensmaker's equation*.

For a first-order substitution of the lensmaker's equation, the lens is assumed to be submerged in air and approximated to be a thin lens. This allows the index of refraction, n_0 , to be assumed to be 1 and the thickness, t , is assumed to be 0, resulting in the simplified equation:

$$\phi = \frac{1}{f} \approx (n - 1) \cdot \left(\frac{1}{R_1} - \frac{1}{R_2} \right)$$

A first-order optical system modeled with thin lenses require the focal power of each element to be defined. The system can then be modeled in a first-order by applying the lensmaker's equations to determine the approximate curvature and refractive index of the lens elements.

A second simplification used for this first-order analysis of an optical system is a small angle approximation. When ray tracing, *Snell's law* will be implemented to determine how much diffraction will be experienced by each ray at a surface. Snell's law describes the phenomena of the change a ray slope will experience at a boundary between two different media. The law states that:

$$n_1 \sin\theta_1 = n_2 \sin\theta_2$$

where n_1 is the incident ray index of refraction, θ_1 is the incident angle, n_2 is the refracted index of refraction, and θ_2 is the resulting refracted angle.

For rays that are traced near the optical axis, which experience a small amount of change, it can be approximated that

$$\sin\theta \approx \theta$$

to allow the calculations to be simplified and provide more rays to be traced with a reduction in computational power. This can be shown to be acceptable for a range of small angles based on the Taylor series expansion of the a sine function:

$$\sin\theta = \sum_{n=0}^{\infty} \frac{(-1)^n \theta^{2n+1}}{(2n+1)!} = \theta - \frac{\theta^3}{3!} + \frac{\theta^5}{5!} + \dots$$

where the *first order* term in the Taylor series expansion is used, and the higher order terms are neglected because they have less impact in reducing the error in the approximation.

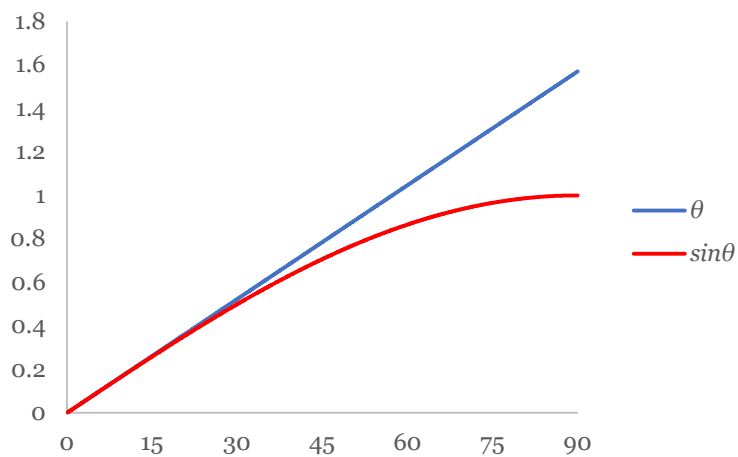


Figure 3: Illustration of divergence between θ and $\sin\theta$ from 0° to 90°

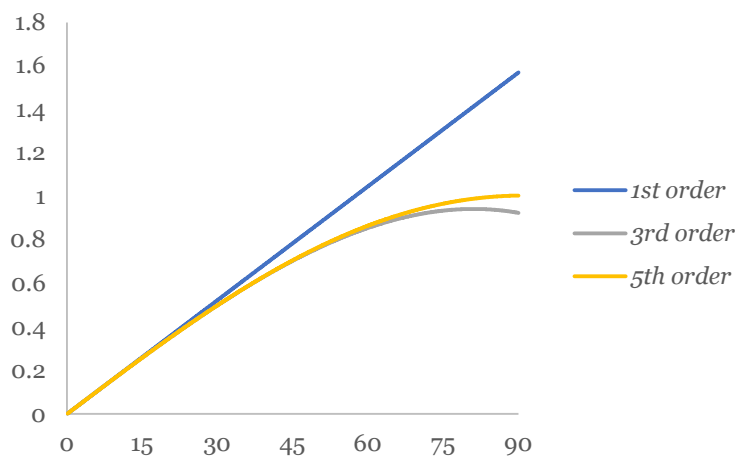


Figure 4: Illustration of divergence between first, third, and fifth order Taylor series expansion for $\sin\theta$ from 0° to 90°

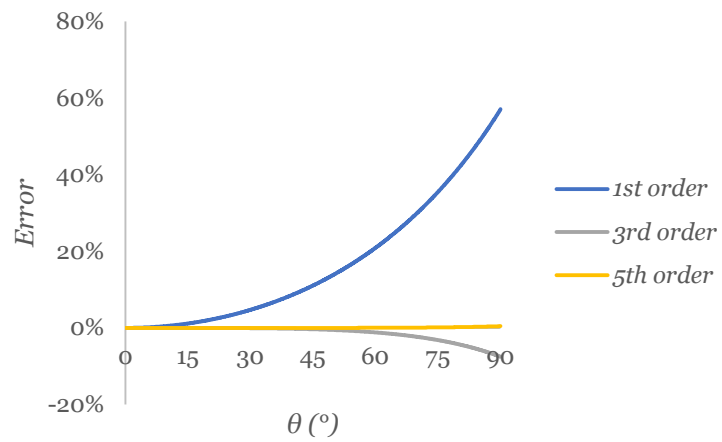


Figure 5: Illustration of percentage error between first, third, and fifth order Taylor series expansion for $\sin\theta$ from 0° to 90°

2.1 Telecentric First-Order Analysis

An *image-space telecentric* system is simulated using an ideal surface. The exit pupil is located at infinity by placing the aperture stop at the front focal plane. Three field angles were used and the system was optimized to have the chief ray exit the system parallel to the optical axis.

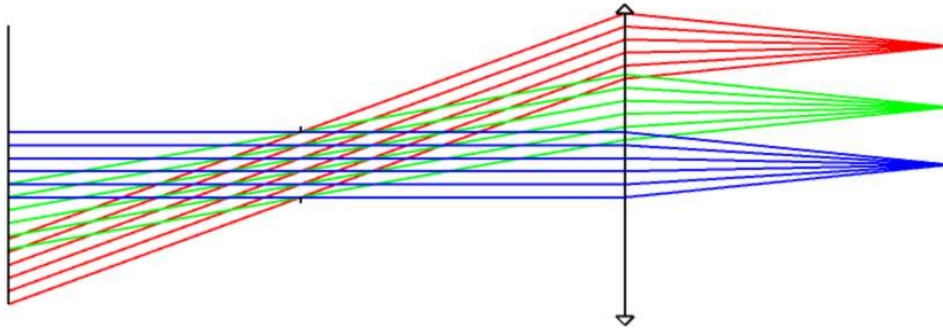


Figure 6: First-order model of an Image-Space Telecentric system

The *image-space telecentric* ideal model demonstrates similar properties to a first-order relay system where the distance from the stop, the image plane, and the focal length of the system are equal. With a first-order lens modeled, all the properties of a telecentric system are ideally demonstrated.

To expand on this approximation, a *double-sided telecentric* system can be modeled through symmetry by having a second first-order system mirrored about the stop.

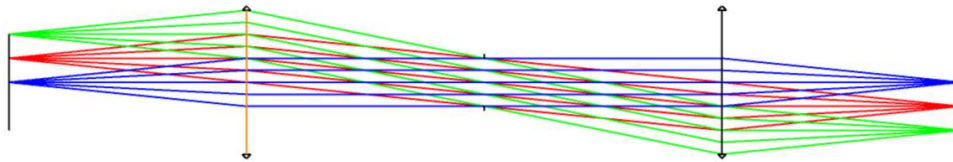


Figure 7: First-order model of a Double-Sided Telecentric system

Through a first-order analysis, an *object-space telecentric* system and *image-space telecentric* system have the same but opposite influence with respect to the system stop, and allows a *double-sided telecentric* system to be modeled as a concatenation of the two

systems. The analysis of single configuration systems can be used to infer that any *image-space telecentric* system would be able to expand to a *double-sided telecentric* through symmetry.

2.2 Multi-configuration Telecentric First-Order Analysis

To make the telecentric system multi-configuration, two thin lenses will be used in the simulation. The distance between lenses will be varied to provide a variable focal length. The system will be optimized to achieve a desired focal length as well as maintaining telecentricity.

Initially, the power of the lenses will be chosen to limit the Petzval curvature present in the system. Petzval field curvature is an optical aberration resulting from the departure of the image surface from a plane to a curved surface. Each element in an optical system contributes to field curvature with its power and thickness. In a system with multiple lenses their properties can be combined to determine the *Petzval sum*, which if zero, results in a system which will have the same optical path length across the aperture or field of view. For thin lenses, the Petzval sum is:

$$\frac{1}{\rho'_k} = - \sum \frac{\phi}{n}$$

Two thin lenses with opposing powers, i.e. powers that sum to zero, allow for a demonstration of a multi-configuration optical system which will have a Petzval sum of zero at the image plane. It can be a good practice to consider this at the first-order analysis of any system to avoid confronting minimizing Petzval field curvature later in the design.

There are two ways of arranging the two lenses to have a sum of zero power, Negative-Positive (N-P) and Positive-Negative (P-N).

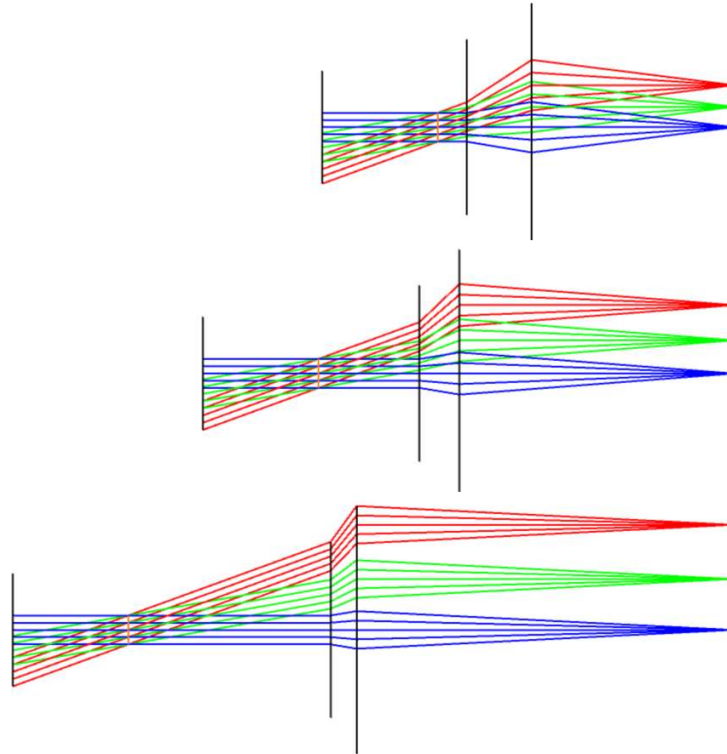


Figure 8: First-order model of a zoom a N-P Image-Space Telecentric zoom system with 40° field of view, with an effective focal length of 200 (top), 325 (middle), and 500 mm(bottom)

The lenses are modeled as a negative lens with a focal length of -150 mm, and a positive lens with a focal length of $+150$ mm. The system is defined with an aperture of 50 mm, and a 40° field of view. The multi-configuration system has an effective focal length of 200 , 325 , and 500 mm, or a 2.5 zoom ratio. The effective focal length is controlled by the spacing between the lenses, and the telecentricity is maintained by the position of the stop.

The system is also demonstrated after changing the orientation from N-P to P-N with all other aspects of the system maintained. A similar result was achievable by varying the distance between the lenses and the position of the stop, however the rays experience sharper transitions by converging after the positive lens which increases the

magnitude of aberrations compared to smoother transition of the diverging rays in the N-P configuration.

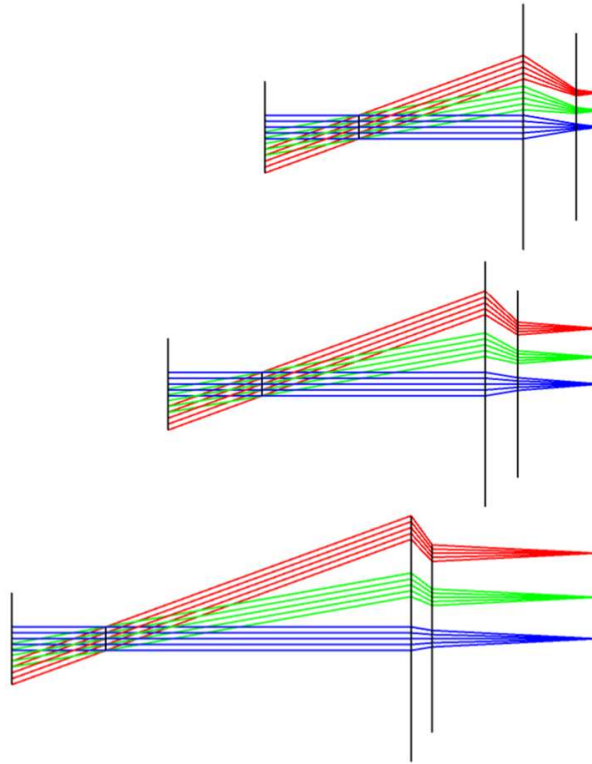


Figure 9: First-order model of a zoom a P-N Image-Space Telecentric zoom system with 40° field of view, with an effective focal length of 200 (top), 325 (middle), and 500 mm(bottom)

This simulation shows that a telecentric zoom lens can accommodate a change in the focal length of the system while maintaining telecentricity, if the aperture stop is varied as the focal length changes. The system requires two singlets or lens groups which maintain similar focal lengths and vary the distance between the lens groups and the stop.

The original N-P system was modified to have the stop at the rear focal plane to make the system *object-space telecentric*. The effective focal length of 200, 325, and 500 mm was maintained as well as the spacing between the ideal lens surfaces. However, the overall length of the system was increased by the change of the stop position.

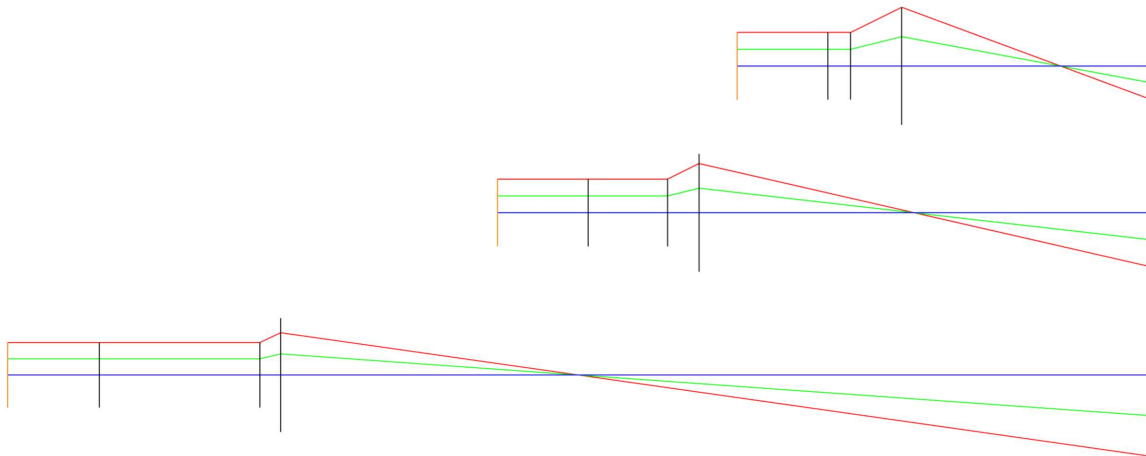


Figure 10: First-order model of a zoom a N-P Object-Space Telecentric zoom system with 40° field of view, with an effective focal length of 200 (top), 325 (middle), and 500 mm(bottom)

An existing zoom lens with a zoom ratio of 3:1 was modeled using first-order lenses. The system consists of two groups of lenses, with the first group providing an effective positive power and the second group an effective negative power, making this system an elaboration of the two element P-N imaging system. These groupings allow the system to have less power on each element and provide a balanced transition and better ability to control aberrations.

To make the first-order system telecentric, the stop position was varied to allow the angular magnification to approach zero. The system was modeled with a 10° field of view which can be seen **Figure 11** that the 75 mm focal length configuration has light filling the lens aperture, and a larger field of view could not be achieved without resulting in vignetting in the image.

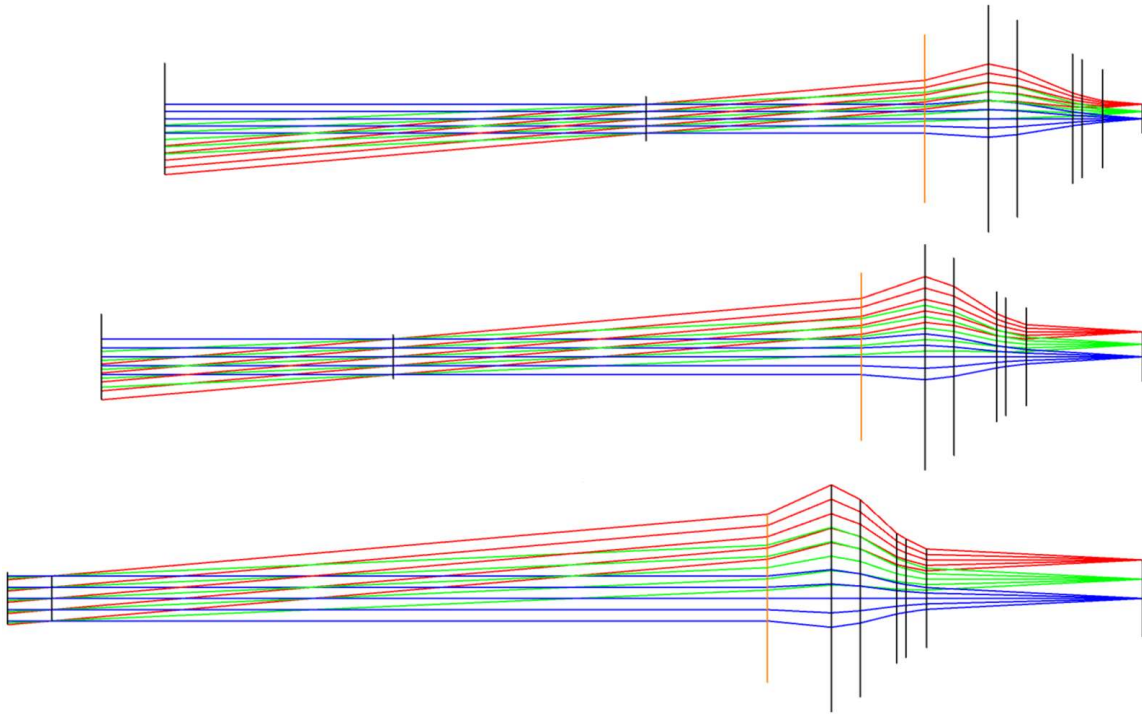


Figure 11: First-order model of a multi-configuration Telecentric system based on an existing zoom system. F/6, F/8, F/10, 10° Field of View, with an effective focal length of 25 (top), 50 (middle), and 75 mm(bottom)

3 Third-Order Analysis

For a third-order analysis, aberrations become a fundamental concern and need to be examined individually. The third-order aberrations will be discussed and explored to better understand the impact they have on the image quality. This analysis will be performed through a numerical approach using an aberration function, and specifically for considerations related to telecentric systems.

The *aberration function*, $W(\vec{H}, \vec{\rho})$, is a mathematical function used for characterizing waveform deformation by providing the optical path length at the exit pupil of a given ray as a function of the normalized field vector, \vec{H} , and the aperture vectors, $\vec{\rho}$. The *aberration function* is a scalar resulting from the dot product of the field and aperture vectors and is invariant of the rotation of the vectors about the optical axis. These aberrations can be classified based on symmetry, either axially symmetric, plane symmetric, and double plane symmetric.

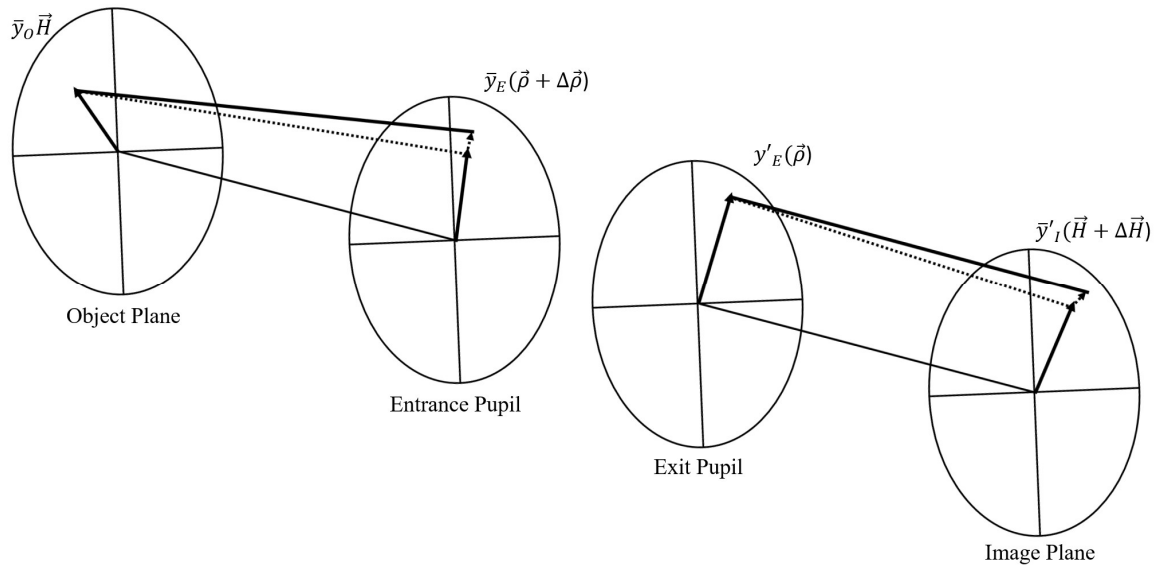


Figure 12: Illustration of optical system with the field vector, \vec{H} , scaled by the chief ray height, \bar{y}_O , at the object plane, and the aperture vector, $\vec{\rho}$, scaled by the marginal ray height, y'_E , at the exit pupil. A first-order ray shown as a dotted line, and the real ray shown as a solid line.

The *aberration function* can be shown in dot product form, as introduced by Roland Shack⁷, to include contributions from the effects of the aberrations present:

$$W(\vec{H}, \vec{\rho}) = \sum_{j,m,n} W_{k,l,m} (\vec{H} \cdot \vec{H})^j (\vec{H} \cdot \vec{\rho})^m (\vec{\rho} \cdot \vec{\rho})^n$$

This dot product form can be expanded to a third order of approximation of the image aberrations:

$$\begin{aligned} W(\vec{H}, \vec{\rho}) = & W_{000} + W_{200}(\vec{H} \cdot \vec{H}) + W_{111}(\vec{H} \cdot \vec{\rho}) + W_{020}(\vec{\rho} \cdot \vec{\rho}) \\ & + W_{040}(\vec{\rho} \cdot \vec{\rho})^2 + W_{131}(\vec{H} \cdot \vec{\rho}) \cdot (\vec{\rho} \cdot \vec{\rho}) + W_{222}(\vec{H} \cdot \vec{\rho})^2 \\ & + W_{220}(\vec{H} \cdot \vec{H}) \cdot (\vec{\rho} \cdot \vec{\rho}) + W_{311}(\vec{H} \cdot \vec{H}) \cdot (\vec{H} \cdot \vec{\rho}) \\ & + W_{400}(\vec{H} \cdot \vec{H})^2 \end{aligned}$$

which accounts:

W_{000}	Uniform piston
W_{200}	Standard piston
W_{111}	Magnification
W_{020}	Focus
W_{040}	Spherical aberration
W_{131}	Coma
W_{222}	Astigmatism
W_{220}	Field curvature
W_{311}	Distortion

The transverse ray aberration is a mathematical function for determining the change in the distance between the first-order ray and the real ray, orthogonally, along the optical axis. The transverse ray aberration is defined as:

⁷ Sasián, José. *Introduction to Aberrations in Optical Imaging Systems* (Cambridge, UK, Cambridge University Press, 2013)

$$\vec{\varepsilon} = \frac{1}{n'u'} \vec{\nabla}_\rho W(\vec{H}, \vec{\rho})$$

and provides a vector which illustrates axial impact of the aberration function on an image.

3.1 Spherical Aberration

Spherical aberration is an axially symmetric aberration and is the result of a difference between where the marginal ray and chief ray come to focus. Spherical aberration has the aberration function:

$$W_{040}(\vec{\rho} \cdot \vec{\rho})^2$$

An optical system with spherical aberration has a ray caustic where the rays come to focus along the z-axis, with a nominal paraxial focus, minimum RMS spot size, minimum circle, and marginal focus. With proper understanding of the ray caustic, defocus can be introduced into the optical system to provide the best compensation to spherical aberration.

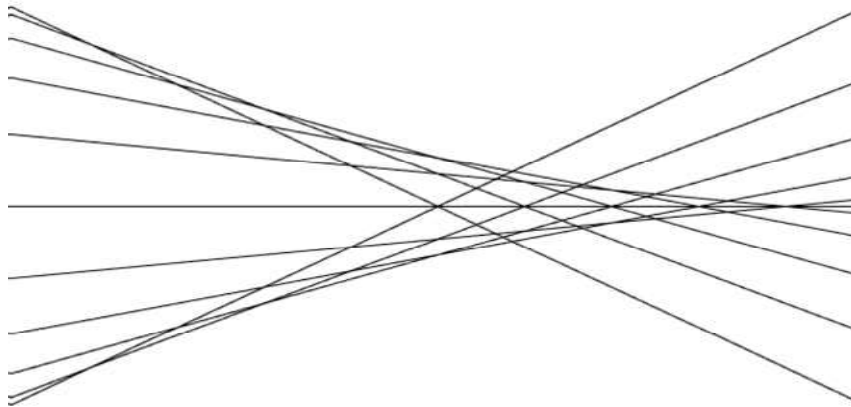


Figure 13: Example of a ray caustic resulting from Spherical Aberration.

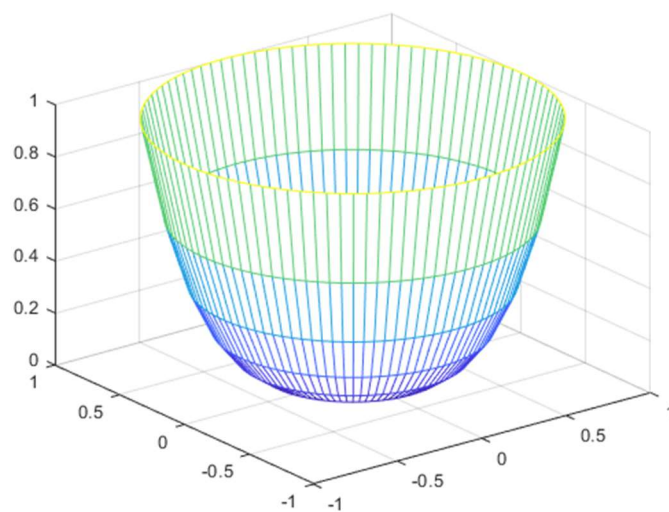


Figure 14: Visualization of the waveform deformation resulting from Spherical Aberration.

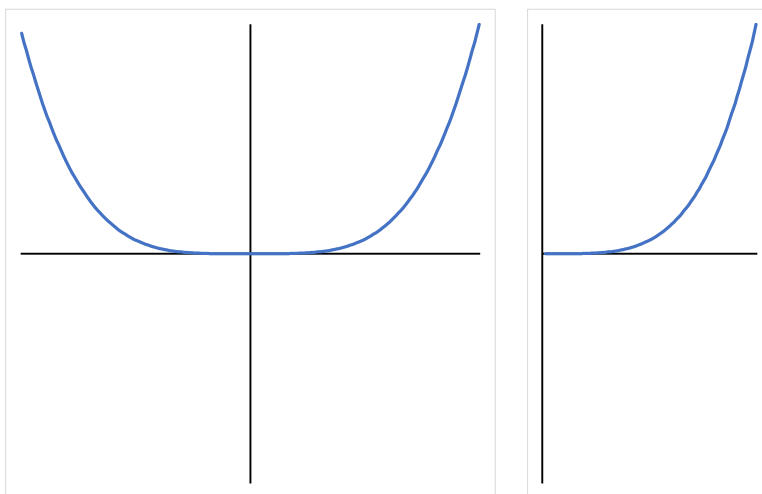


Figure 15: Transverse ray plot of Spherical Aberration.

3.2 Coma

Coma aberration is a plane symmetric aberration, which is an off-axis aberration, where annual zones have different magnifications resulting in a point that looks like a comet. Coma aberration has the aberration function:

$$W_{131}(\vec{H} \cdot \vec{\rho}) \cdot (\vec{\rho} \cdot \vec{\rho})$$

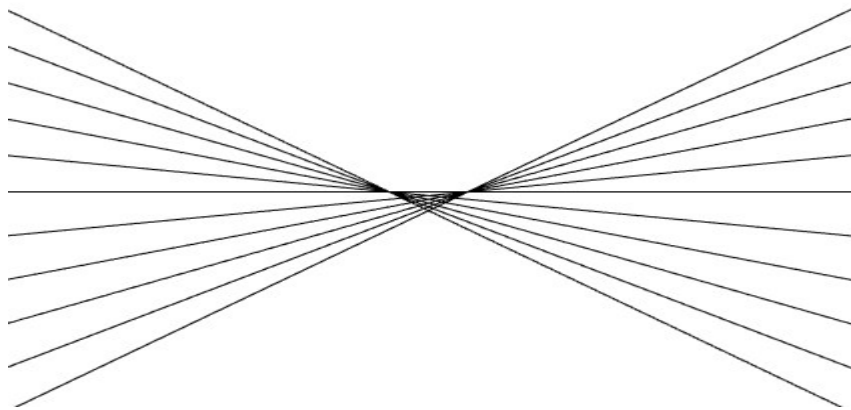


Figure 16: Example of a ray caustic resulting from Coma Aberration.

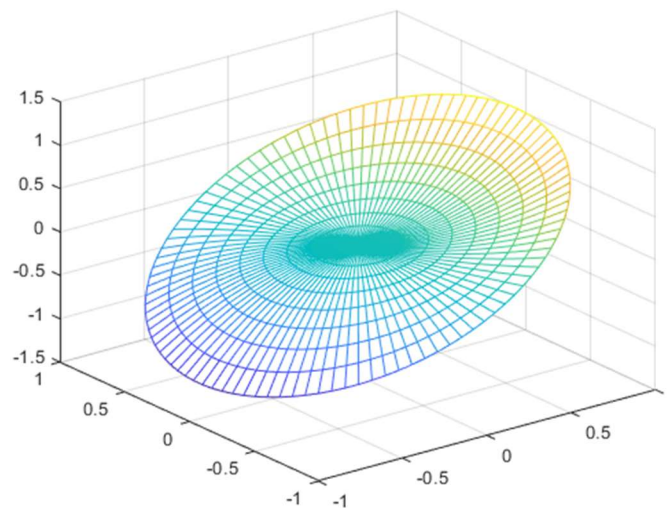


Figure 17: Visualization of the waveform deformation resulting from Coma Aberration.

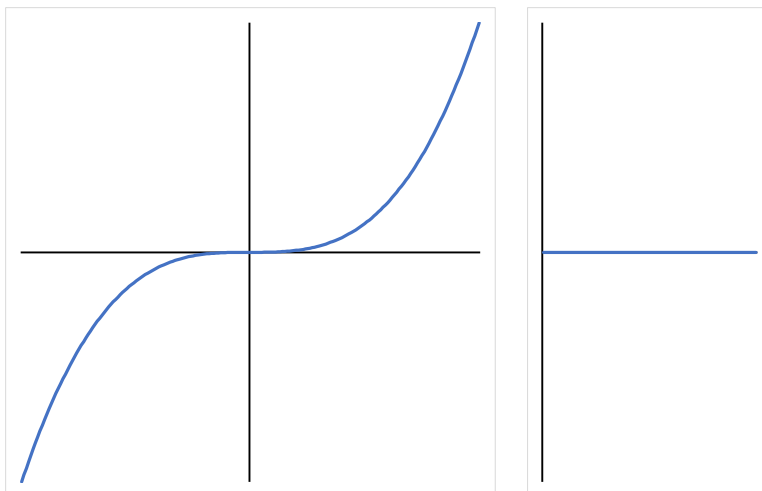


Figure 18: Transverse ray plot of Coma Aberration.

3.3 Astigmatism

Astigmatism aberration is a double plane symmetric aberration resulting from a meridian ray fan coming to focus at one point with a second orthogonal ray fan coming to focus at a different point. Astigmatism aberration has the aberration function:

$$W_{222}(\vec{H} \cdot \vec{\rho})^2$$

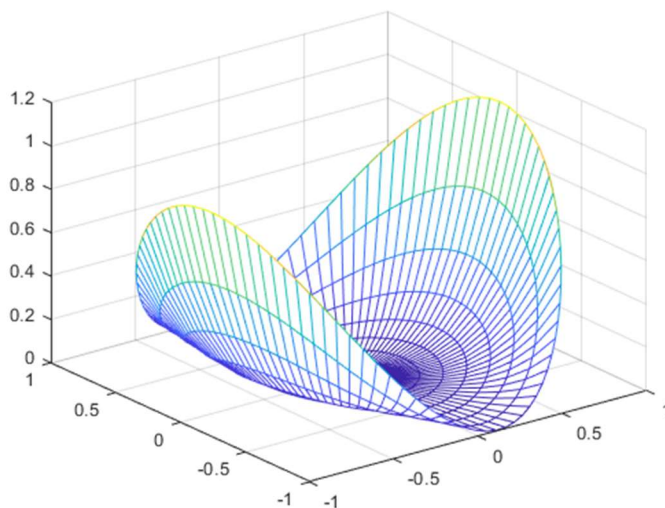


Figure 19: Visualization of the waveform deformation resulting from Astigmatism.

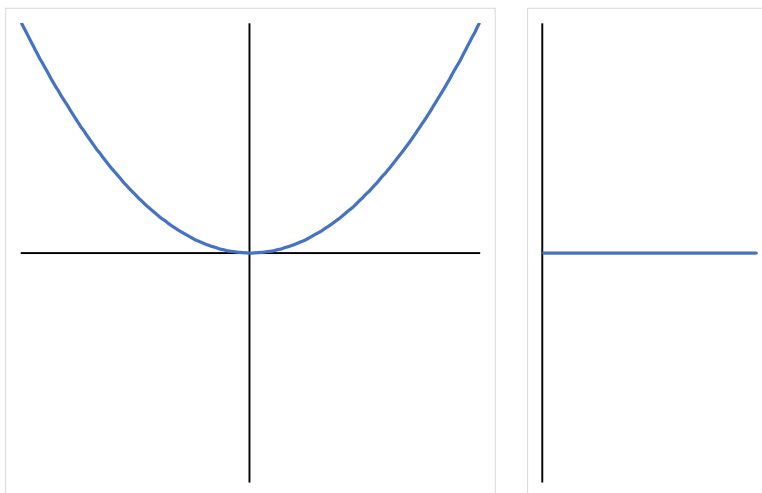


Figure 20: Transverse ray plot of Astigmatism.

3.4 Field Curvature

Field curvature is an axially symmetric aberration of an optical system where there is a deviation from imaging to a plane, such as imaging to a curved surface. This is defined by the departure from the ideal image plane to the image surface measured axially and known as the Petzval radius. Field curvature is a radially symmetric aberration which increases quadratically as a function of the field of view and has the aberration function:

$$W_{220}(\vec{H} \cdot \vec{H}) \cdot (\vec{\rho} \cdot \vec{\rho})$$

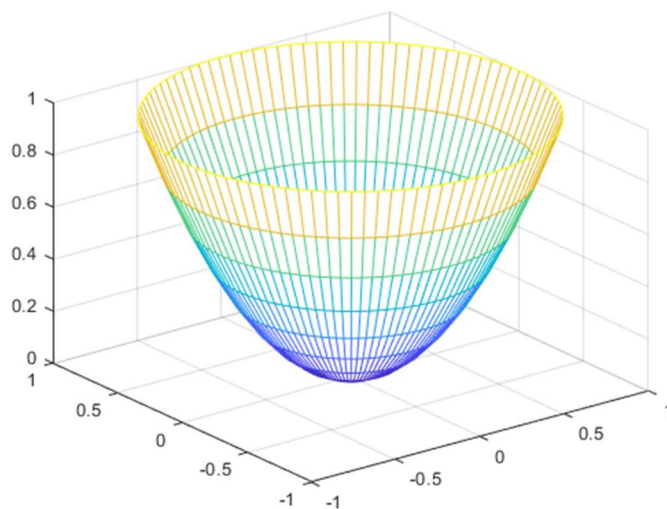


Figure 21: Visualization of the waveform deformation resulting from Field curvature.

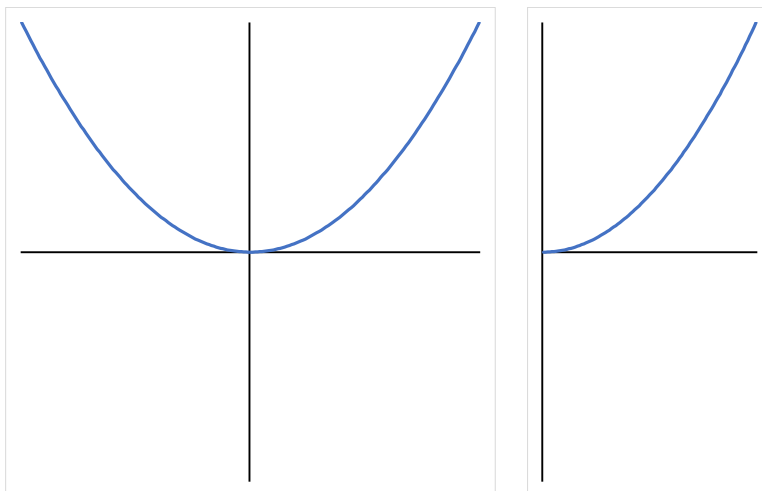


Figure 22: Transverse ray plot of Field curvature.

3.5 Distortion

Distortion is a plane symmetric aberration where the magnification of the optical system varies across the field of view. Distortion has the aberration function:

$$W_{311}(\vec{H} \cdot \vec{H}) \cdot (\vec{H} \cdot \vec{\rho})$$

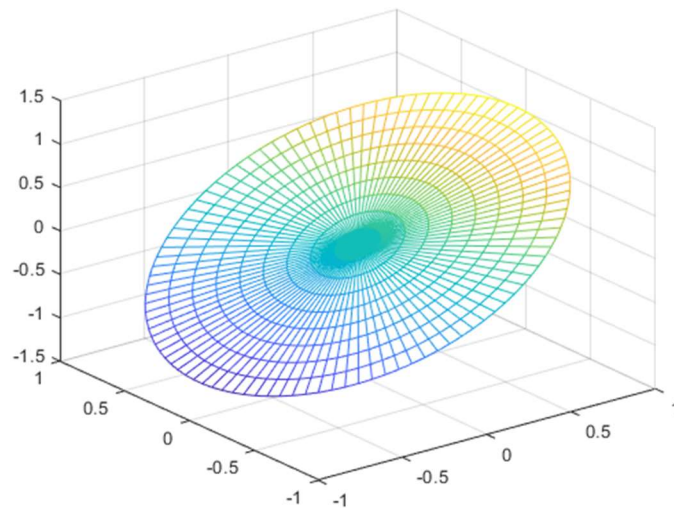


Figure 23: Visualization of the waveform deformation resulting from Distortion.

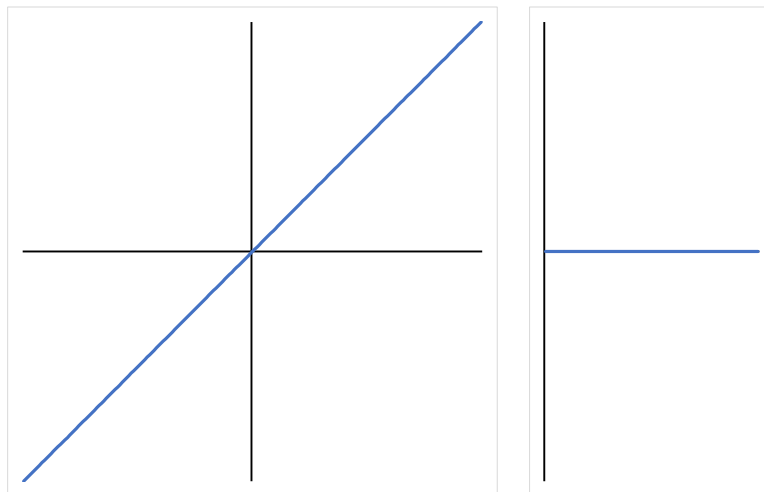


Figure 24: Transverse ray plot of Distortion.

Distortion results from an image of an off-axis point that is formed closer to or farther from the axis than the image height in the first-order expression. The change in the height

of an ideal image in the first-order to the real image height can be expressed as a percentage change. For the image of an object that is located at infinity, the image height can frequently be modeled as:

$$\bar{Y}_l = f \tan(\theta)$$

where the image height is a function of the field of view. This is a common occurrence for distortion in optical systems but is not always the case.

The throughput of an optical system, or *etendue*, ε , measures the capacity of an optical system. The etendue of an optical system is the product of the area of the pupil and the solid angle of the field of view, or the product of the detector area and the speed of the lens. The etendue in object space is defined as:

$$\varepsilon = \pi^2 y_e^2 \sin^2(\theta)$$

For a telecentric system, where: $\bar{u} = 0$, the etendue in image space becomes⁸:

$$\varepsilon' = \frac{\pi^2 Y_i^2 y_e^2}{f'^2}$$

If the etendue of the telecentric system is conserved, and no light is lost, then: $\varepsilon = \varepsilon'$ and the distortion on the system has a mapping relationship:

$$\bar{Y}_l = f \sin(\theta)$$

⁸ Sasián, José. *Introduction to Lens Design* (Cambridge, UK, Cambridge University Press, 2019)

3.6 Chromatic Aberrations

The index of refraction of materials varies for different wavelengths of light. This results in a change of optical power for a lens or system as a function of different wavelengths. For example, if the index of refraction is higher for short wavelengths, blue light would come to focus at a shorter distance than red light. This longitudinal axial chromatic aberration is known as chromatic change of focus, $\delta_\lambda W_{020} \rho^2$. When a lens system forms images at different sizes for different colors where there is a lateral chromatic aberration, it is known as chromatic change of magnification, $\delta_\lambda W_{111} H \rho \cos(\phi)$.

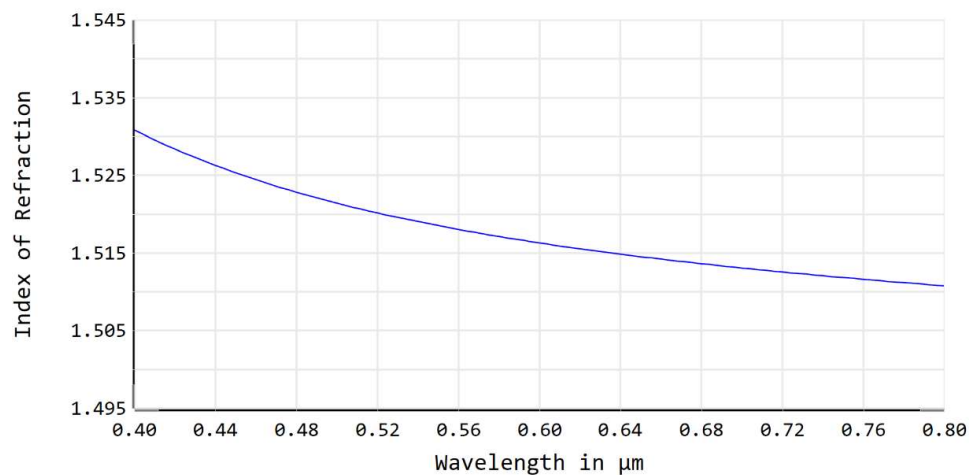


Figure 25: Dispersion Diagram for the index of refraction of N-BK7 glass against wavelength in the visible spectrum.

Each material has a unique dispersion response. For convenience, types of glass are generally categorized by a relative dispersion. The relative dispersion of a glass can be denoted by the Abbe V-number, where three visible wavelengths are used to characterize the glass's dispersion as:

$$V = \frac{n_d - 1}{n_F - n_C}$$

where d , F , and C refer to the Fraunhofer wavelengths: 587.6, 486.1, and 656.3 nm respectively.

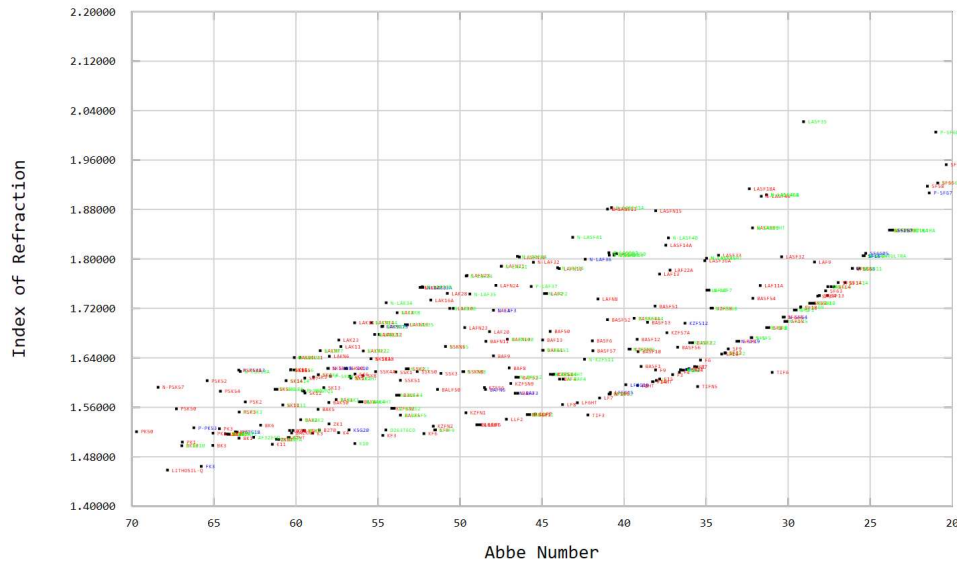


Figure 26: A glass map of different catalogs of manufacturers' glass plot with Index of Refraction against Abbe Number

Chromatic aberration can be corrected by combining two lenses with different glasses, for example, a positive lens with a low relative dispersion and a negative lens with a high relative dispersion. Low dispersive materials are known as crown glasses in contrast to the high dispersive flint glasses. With proper compensating powers between two glasses, a crown and a flint can accommodate the same focal distance for two wavelengths, these lens groups are known as achromatic lenses. Additional corrections can be made to correct for three or more wavelengths providing an apochromatic lens by analyzing the partial dispersion of the glasses.

3.7 Pupil Aberrations

In addition the previously discussed aberrations, which form at the image plane, aberrations can form at the entrance and exit pupils of an optical system. In the same way an object and image plane are conjugate in an imaging system, the entrance and exit pupil are also conjugate. If two optical systems are concatenated the exit pupil of one system requires strict alignment to the entrance pupil of the second system. The optical power, ϕ , of the combination of two optical systems A and B submerged in air is given by:

$$\phi = \phi_A + \phi_B - t\phi_A\phi_B$$

Where the spacing, t , between the groups can be continuously varied in a zoom system. Misalignment of these groups will result in pupil aberrations. Third-order pupil aberrations are related to the previously defined image aberrations and are expressed in an *aberration function*. This pupil aberration function is distinguished from the image aberration function by denoting it as \bar{W} .

Modular lens design provides benefits to designers by allowing the design of lens groups to be modeled and optimized separately. Modular lenses have also been made commercially available, allowing users to combine lens groups in a “mix and match” fashion to have more control over the specifications of the optical system⁹. Modular lens design has a higher potential for misalignment of the pupil, allowing for pupil aberrations to be present. Zoom lenses have higher susceptibility to pupil misalignment as the positions of the lens groups are required to move.

The pupil aberrations are defined in the *pupil aberration function* and can be expanded to a third order of approximation:

⁹ Chang, Matthew, "Pupil aberration in modular zoom lens design," Ph.D. dissertation, College of Optical Sciences, University of Arizona, AZ, USA, 1998 [Online].

$$\begin{aligned}
\bar{W}(\vec{H}, \vec{\rho}) = & \bar{W}_{000} + \bar{W}_{200}(\vec{\rho} \cdot \vec{\rho}) + \bar{W}_{111}(\vec{H} \cdot \vec{\rho}) + \bar{W}_{020}(\vec{H} \cdot \vec{H}) \\
& + \bar{W}_{040}(\vec{H} \cdot \vec{H})^2 + \bar{W}_{131}(\vec{H} \cdot \vec{H}) \cdot (\vec{H} \cdot \vec{\rho}) + \bar{W}_{222}(\vec{H} \cdot \vec{\rho})^2 \\
& + \bar{W}_{220}(\vec{H} \cdot \vec{H}) \cdot (\vec{\rho} \cdot \vec{\rho}) + \bar{W}_{311}(\vec{\rho} \cdot \vec{\rho}) \cdot (\vec{H} \cdot \vec{\rho}) \\
& + \bar{W}_{400}(\vec{\rho} \cdot \vec{\rho})^2
\end{aligned}$$

Pupil spherical aberration, \bar{W}_{040} , causes a lateral shift at the pupil for different field points. This can result in vignetting in the system and an annular obscuration typically described as the “kidney bean effect” because of the visual shape of the aberration in imaging systems. This is related to the image wave aberration of quartic piston:

$$\bar{W}_{040} = W_{400}$$

Pupil coma aberration, \bar{W}_{131} , causes the ray bundle at the pupil to be anamorphically distorted, resulting in an unequal magnification along the optical axis. This can be related to image wave aberrations as:

$$\bar{W}_{131} = W_{311} + \frac{1}{2}\mathcal{K} \cdot \Delta\{\bar{u}^2\}$$

where, \mathcal{K} , is the Lagrange invariant, and expresses the etendue of a lens or system independent on the plane it is calculated. The Lagrange invariant is a first-order quantity and is defined as:

$$\mathcal{K} = n\bar{u}y - n\bar{u}y$$

Pupil distortion is an aberration resulting from a mismatch in the size of the complimentary pupil, where the exit pupil is larger than the entrance pupil and results in vignetting. Pupil distortion is related to image coma as:

$$\bar{W}_{311} = W_{131} + \frac{1}{2}\mathcal{K} \cdot \Delta\{u^2\}$$

Pupil astigmatism, \bar{W}_{222} , and pupil field curvature, \bar{W}_{220} , are related to their respective image aberration with the relationship:

$$\bar{W}_{222} = W_{222} + \frac{1}{2}\mathcal{K} \cdot \Delta\{u\bar{u}\}$$

$$\bar{W}_{220} = W_{220} + \frac{1}{4} \mathcal{K} \cdot \Delta\{u\bar{u}\}$$

Finally, pupil quartic piston aberration resulting from a misalignment between the entrance and exit pupils and relates to image spherical aberration as:

$$\bar{W}_{400} = W_{040}$$

In the case of a telecentric system, the chief ray entering or exiting the optical system is parallel to the optical axis described as: $\bar{u} = 0$. This results in a condition where the aberrations for pupil coma, pupil astigmatism and pupil field curvature act effectively as image aberrations:

$$\bar{W}_{131} = W_{311}$$

$$\bar{W}_{222} = W_{222}$$

$$\bar{W}_{220} = W_{220}$$

leaving only pupil spherical aberration and pupil distortion as the pupil aberrations¹⁰.

To understand the impact of aberrations on the performance of a telecentric lens, it would be useful to have a metric for the degree of telecentricity of a system. This measurement of the degree of telecentricity would effectively be the chief ray slope error, or the change in the chief ray slope, $\Delta\bar{u}$. With no errors from other aberrations present in the system, an expression can be derived from the remaining aberrations to calculate the degree of telecentricity.

¹⁰ Sasián, José. *Introduction to Lens Design* (Cambridge, UK, Cambridge University Press, 2019)

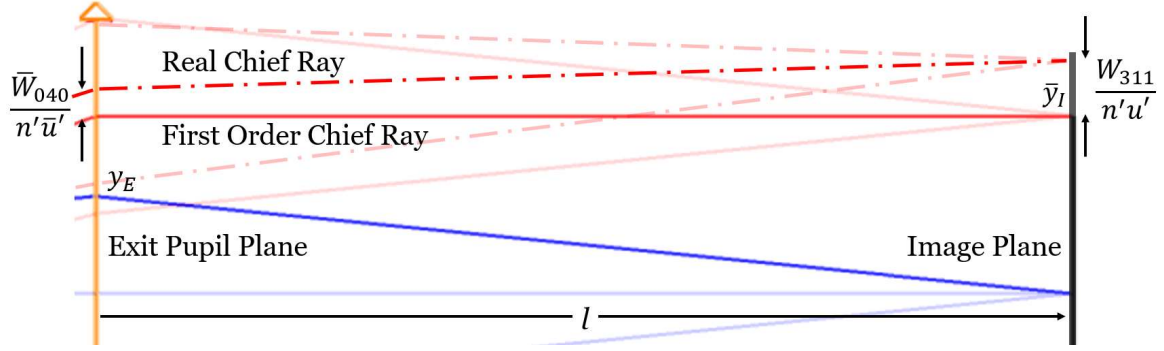


Figure 27: Illustration of the wandering pupil and the difference between the First Order Chief Ray compared to Real Chief Ray resulting from the aberrations present in the system.

The pupil spherical aberration resulting from a wandering pupil results in an offset at the exit pupil plane and the distortion results in an offset at the image plane. The change in the chief ray angle can be approximated as the ratio of the difference between the offsets and the distance between the exit pupil and the image plane.

$$\Delta\bar{u} = \frac{\Delta\bar{e}}{l}$$

The contribution from the pupil spherical aberration is a function of the gradient of the aberration with respect to the field vector:

$$\frac{1}{n'u'} \vec{\nabla}_H \bar{W}_{040} H^4$$

And the contribution from the distortion is a function of the gradient of the aberration with respect to the pupil vector:

$$\frac{1}{n'u'} \vec{\nabla}_\rho W_{311} H^3 \rho \cos\theta$$

The resulting expression can be used to describe how well a system maintains telecentricity and will be useful for evaluating multi-configuration systems at different positions.

$$\Delta\bar{u} = \frac{1}{n'} \left(\frac{4 \cdot \bar{W}_{040}}{\bar{y}_I} - \frac{W_{311}}{y_E} \right)$$

4 Third-Order Zoom Lens Design

Following a third-order aberration analysis, multi-configuration lenses were then modeled as telecentric systems to analyze the performance and the necessary compromises to maintain telecentricity. The third order optical systems were modeled using the optical design software OpticStudio 20.2.2, which provides comprehensive analysis tools for evaluation of expected image quality. Additional analysis was then performed to determine the degree of telecentricity of the systems and how it varies throughout the zoom range.

Two studies were performed to demonstrate the process of modeling and analyzing telecentric multi-configuration systems. The first is a sample zoom lens which is included with OpticStudio as a demonstration tool for multi-configuration settings, it is an F/5-F/7.8 lens with a variable focal length of 29 – 78 mms and a field of view of 11.4°. The second is a NIKKOR telephoto camera lens referenced from Nikon Corporation US patent 5,126,883, which operates at F/4 with a 62 – 167 mm focal length and a field of view of 12°.

4.1 Study 1

A sample lens from OpticStudio was evaluated as a candidate for a basis for a telecentric zoom lens. The sample zoom lens was chosen for the position of the stop, the zoom range, and the aberration correction. The lens includes three lens groups with two variable separations between them, three aspheric surfaces, and the ability to accommodate an 11.4° field of view.

The lens was analyzed with no modifications to have an understanding of the innate image quality and performance. The image quality was quantified by the ray fans and field curvature for three wavelengths: 486, 588, and 656 nm, three field angles: 0.0° , 4.1° , and 5.8° , and at three focal lengths: 25, 50, and 75 mm.

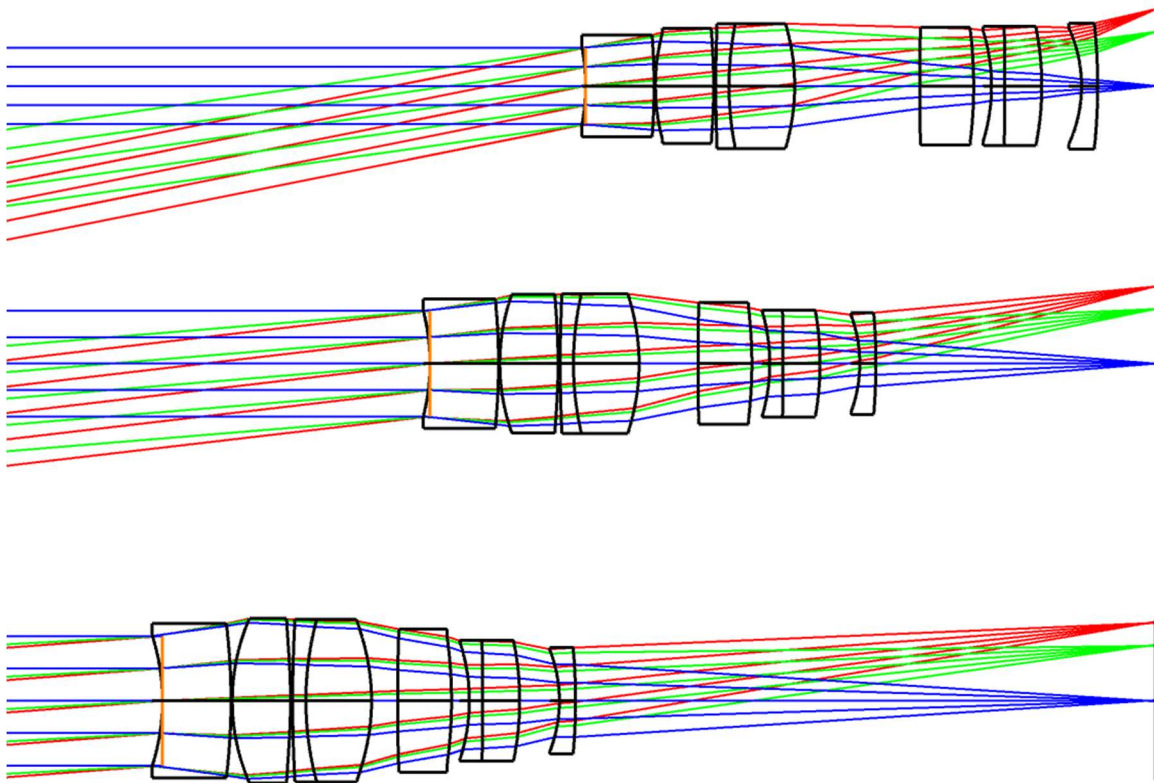


Figure 28: Multi-configuration zoom lens. F/5, F/6.2, F/7.8, 11.6° Field of View, with an effective focal length of 25 (top), 50 (middle), and 75 mm (bottom)

Radius	Thickness (mm)	Refractive Index	Abbe No.
-16.20	5.18	1.77	4.96
-48.88	0.10		
15.67	4.40	1.53	4.91
-42.96	0.16		
108.70	1.00	1.81	2.54
23.62	4.96	1.49	7.02
-16.06	d_1		
-425.53	4.04	1.49	7.02
-35.44	1.35		
-14.15	1.00	1.71	5.38
-251.26	2.80	1.76	2.71
-22.50	3.00		
-10.58	1.22	1.78	4.96
-44.44	d_2		

Table 1: Prescription for a sample zoom lens. F/5, F/6.2, F/7.8, 11.6° Field of View, and an effective focal length of 25, 50, and 75 mm.

Variable	Config 1	Config 2	Config 3
d_1	9.48	4.48	2.00
d_2	4.47	21.21	43.81

Table 2: Addendum to the prescription for the sample zoom lens showing the multi-configuration distances between lens groups.

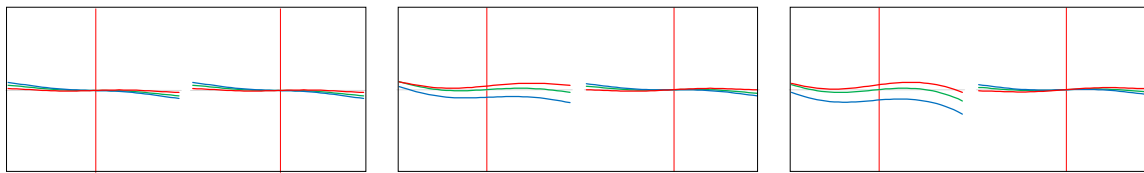


Figure 29: Tangential and Sagittal ray fan of sample zoom lens, with a field of 0.0° at a focal length of 25, 50, and 75 mm, from left to right, using a scale of $\pm 100.0 \mu\text{m}$.

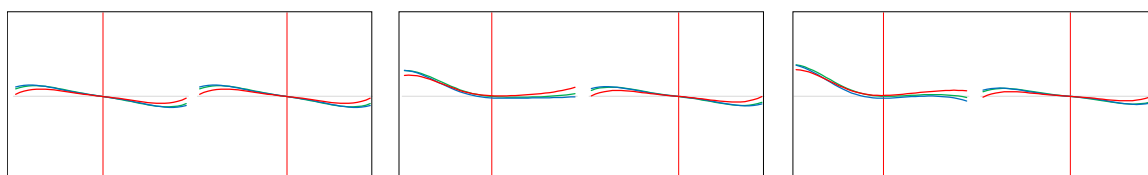


Figure 30: Tangential and Sagittal ray fan of sample zoom lens, with a field of 4.1° at a focal length of 25, 50, and 75 mm, from left to right, using a scale of $\pm 100.0 \mu\text{m}$.

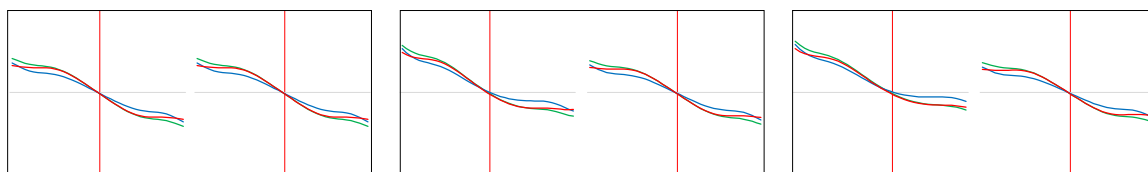


Figure 31: Tangential and Sagittal ray fan of sample zoom lens, with a field of 5.8° at a focal length of 25, 50, and 75 mm, from left to right, using a scale of $\pm 100.0 \mu\text{m}$.

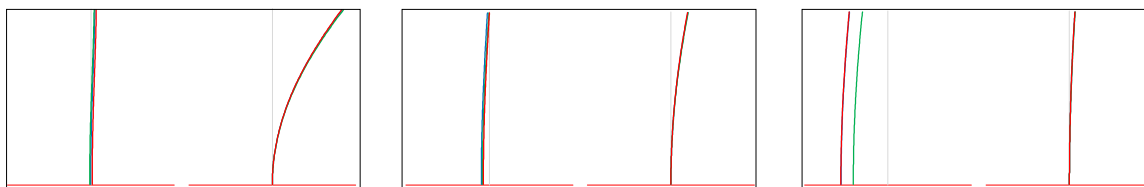


Figure 32: Field curvature and distortion plots of sample zoom lens, at a focal length of 25, 50, and 75 mm from left to right, using a scale of $\pm 2.0 \text{ mm}$ and $\pm 1.0 \%$.

The lens movement accommodates a zoom ratio of 3 and maintains image quality with aberrations of consistent magnitude throughout the zoom range. The performance for image quality is diminished for a wider field angle and peaks with $\pm 50.0 \mu\text{m}$ of aberrations and nearly 1 mm of field curvature at the longer focal length. And the mechanical simplicity of the design of this system with two lens groups and two variable distances makes this an attractive subject for analysis.

The lens was then modified to maintain image space telecentricity throughout the zoom range. This was accomplished by varying the position of the stop relative to the front

focal plane. It was optimized using a merit function weighted for reducing the angular magnification of the system for the three configurations. To get an understanding of the impact of stop shifting the other aspects of the lens were not modified. The lens was analyzed with the $F/\#$ number maintained from the non-telecentric analysis, which requires the stop diameter to change with the focal length. This allowed an isolation on the performance of the system as well as the degree of telecentricity which can be achieved. The system operated with the same focal lengths 25, 50, and 75 mm but the field of view was limited to avoid vignetting and ghost images. The largest achievable field of view was 4.0° . The system was analyzed with the same three wavelengths: 486, 588, and 656 nm, three field angles: 0.0° , 1.4° , and 2.0° . and at three focal lengths: 25, 50, and 75 mm.

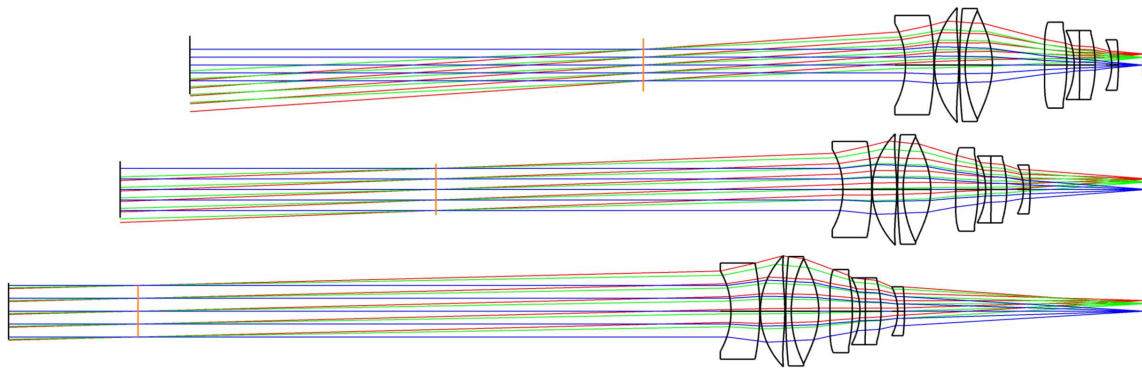


Figure 33: Multi-configuration zoom lens which maintains telecentricity. $F/5$, $F/6$, $F/8$, 4° Field of View, with an effective focal length of 25 (top), 50 (middle), and 75 mm (bottom) with the stop positioned to maintain telecentricity.

Radius	Thickness (mm)	Refractive Index	Abbe No.
Infinity	d_1		
-16.20	5.18	1.77	4.96
-48.88	0.10		
15.67	4.40	1.53	4.91
-42.96	0.16		
108.70	1.00	1.81	2.54
23.62	4.96	1.49	7.02
-16.06	d_2		
-425.53	4.04	1.49	7.02
-35.44	1.35		
-14.15	1.00	1.71	5.38
-251.26	2.80	1.76	2.71
-22.50	3.00		
-10.58	1.22	1.78	4.96
-44.44	d_3		

Table 3: Prescription for Study 1 which maintains telecentricity. F/5, F/6, F/8, 4° Field of View, and an effective focal length of 25, 50, and 75 mm.

Variable	Config 1	Config 2	Config 3
d_1	47.64	73.22	106.71
d_2	9.48	4.48	2.00
d_3	4.47	21.21	43.81

Table 4: Addendum to the prescription for Study 1 showing the multi-configuration distances between lens groups.

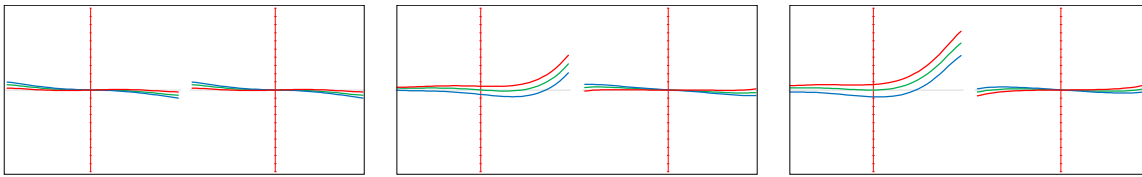


Figure 34: Tangential and Sagittal ray fan of Study 1, with a field of 0.0° at a focal length of 25, 50, and 75 mm, from left to right, using a scale of $\pm 100.0 \mu\text{m}$.

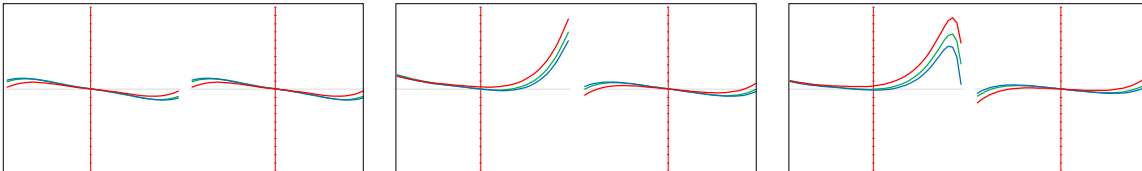


Figure 35: Tangential and Sagittal ray fan of Study 1, with a field of 1.4° at a focal length of 25, 50, and 75 mm from left to right, using a scale of $\pm 100.0 \mu\text{m}$.

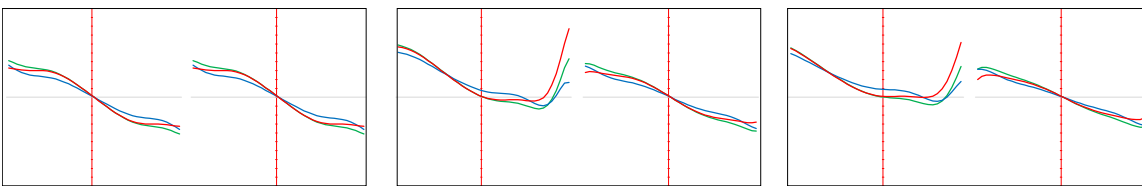


Figure 36: Tangential and Sagittal ray fan of Study 1, with a field of 2.0° at a focal length of 25, 50, and 75 mm from left to right, using a scale of $\pm 100.0 \mu\text{m}$.

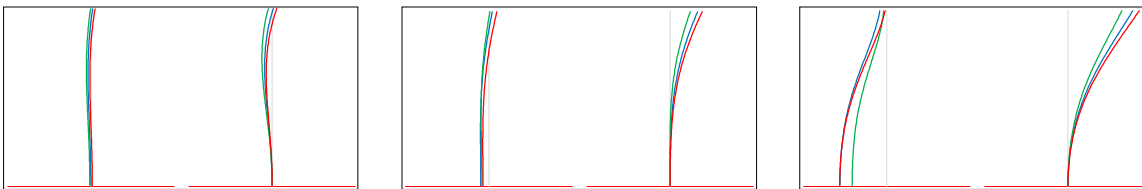


Figure 37: Field curvature and distortion plots of Study 1, at a focal length of 25, 50, and 75 mm from left to right, using a scale of $\pm 2.0 \text{ mm}$ and $\pm 1.0 \%$.

	W040	W131	W222	W220P	W311	W020	W111
25 mm	0.5225	2.1419	2.0776	-0.024	1.4436	-0.4981	-2.2864
50 mm	0.7421	1.5016	0.5361	-0.0156	-0.1643	-0.1093	-0.3444
75 mm	-0.8038	-2.5767	-1.9433	-0.0098	-1.4353	1.0643	1.2869

Table 5: Seidel Coefficients for Study 1 showing the impact of each aberration on the system, at a focal length of 25, 50, and 75 mm from top to bottom, expressed in waves.

The image quality resulting from modifying the stop position was reduced with increased magnitude of aberrations, particularly with a longer focal length and at the larger field angles. The field curvature exceeds 1.0 mm at a 75 mm focal length and the distortion nearly reaches 1.0%.

A program, or macro, was written in OpticsStudio to generate a plot of the change in the chief ray angle at the image plane used to express the degree of telecentricity of the system. The macro analyzed the accumulated distortion and pupil spherical aberration by tracing rays through the system across a normalized pupil and through each surface. The source code for the macro can be found in Appendix B.

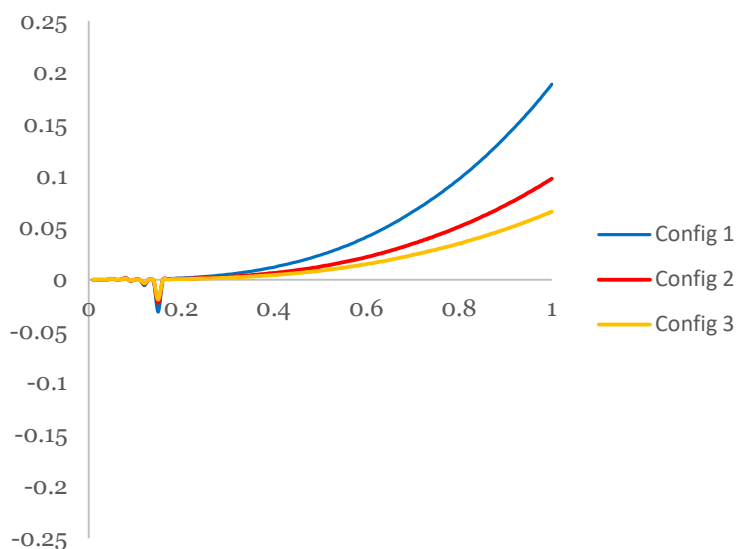


Figure 38: Visualization of the degree of telecentricity of the telecentric zoom lens expressed as a percentage across a normalized pupil.

From this analysis, the degree of telecentricity of this optical system increases as the focal length increases with a maximum of 0.2% at the edge of the field of view. There is a perturbation for all three configurations near the origin.

4.2 Study 2

A second zoom lens was selected to be analyzed for the properties of the described multi-configuration and analyzed in three positions. The lens was detailed in US Patent 5,126,883: *Telephoto Zoom Lens*, by inventors Sato and Hamanishi from the Nikon Corporation of Tokyo, Japan. This zoom lens was selected to analyze in a telecentric configuration because it was an extremely popular consumer photography lens and was designed to provide a telephoto image along the zoom range.

The lens was comprised of five groups of lenses with four mechanical movements and was capable of a focal length which varied from 62 to 168 mm with a field of view of 11.8° to 30.4° at F/4.6. The lens was designed with an emphasis on a large zoom ratio and a relatively compact size and reduced number of elements. Additionally, this system is interesting because it does not use any aspheric surfaces.

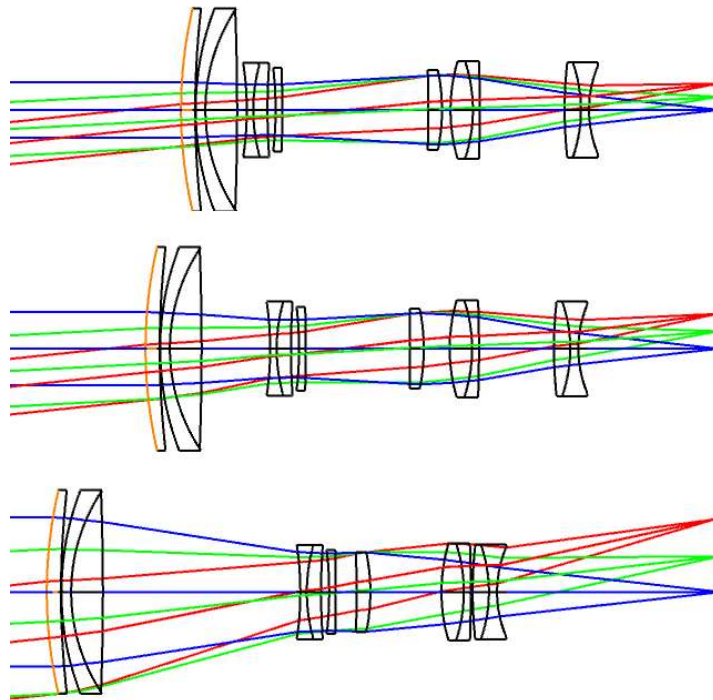


Figure 39: Multi-configuration zoom lens. F/4.6, 12.0° Field of View, with an effective focal length of 62 (top), 82 (middle), and 168 mm (bottom)

Radius	Thickness (mm)	Refractive Index	Abbe No.
Infinity	50.00		
110.67	3.50	1.52	64.10
218.03	0.10		
69.14	2.40	1.81	25.40
44.75	7.80	1.52	64.10
-645.77	d_1		
-76.60	1.60	1.69	50.70
41.75	3.50	1.81	25.40
156.00	2.00		
-87.57	1.60	1.70	55.60
-695.19	d_2		
-840.52	3.43	1.61	58.50
-48.25	d_3	1.76	2.710
42.00	5.50	1.66	57.00
-38.24	1.70	1.81	25.40
-343.79	d_4		
106.73	4.00	1.75	35.20
-35.00	2.00	1.71	5.39
28.12	32.56		

Table 6: Prescription for *US Patent 5,126,833*, which maintains telecentricity. F/4.6, 12° Field of View, and an effective focal length of 62, 82, and 168 mm.

Variable	Config 1	Config 2	Config 3
d_1	2.38	16.88	48.59
d_2	35.91	25.68	5.10
d_3	2.11	6.37	17.51
d_4	20.89	18.47	0.47

Table 7: Addendum to the prescription for *US Patent 5,126,833*, showing the multi-configuration distances between lens groups.

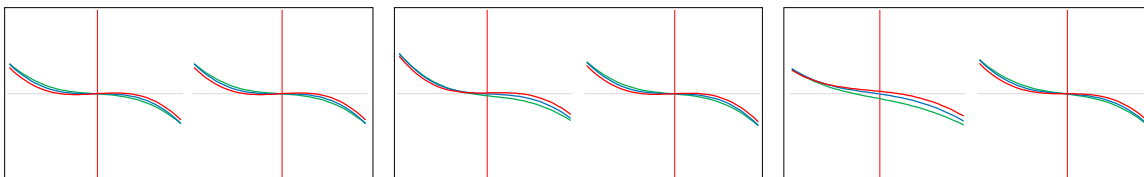


Figure 40: Tangential and Sagittal ray fan of *US Patent 5,126,833*, with a field of 0.0° at a focal length of 62, 82, and 168 mm, from left to right, using a scale of $\pm 200.0 \mu\text{m}$.

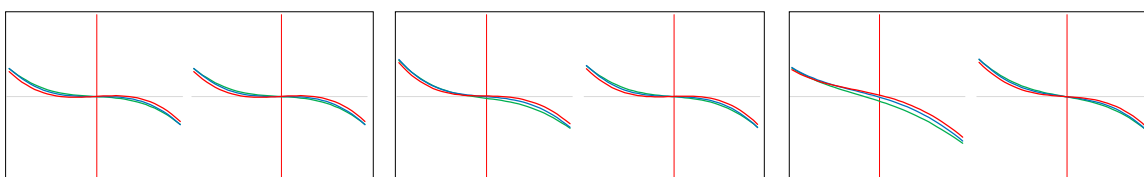


Figure 41: Tangential and Sagittal ray fan of *US Patent 5,126,833*, with a field of 3.0° at a focal length of 62, 82, and 168 mm, from left to right, using a scale of $\pm 200.0 \mu\text{m}$.

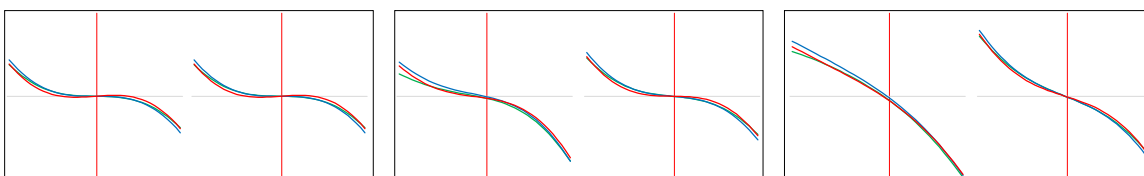


Figure 42: Tangential and Sagittal ray fan of *US Patent 5,126,833*, with a field of 6.0° at a focal length of 62, 82, and 168 mm, from left to right, using a scale of $\pm 200.0 \mu\text{m}$.

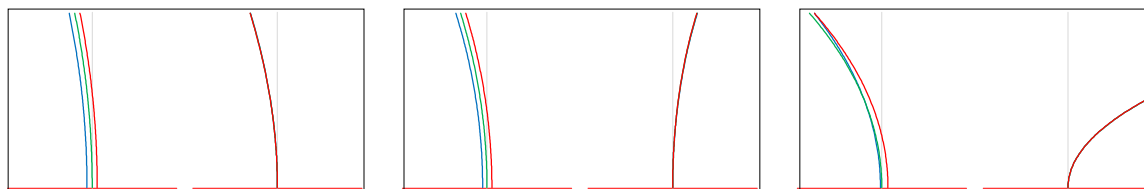


Figure 43: Field curvature and distortion plots of *US Patent 5,126,833*, at a focal length of 62, 82, and 168 mm from left to right, using a scale of $\pm 0.50 \text{ mm}$ and $\pm 1.0 \%$.

The movement of this lens is more complicated than the OpticsStudio lens, which provide a more compact design. With the more complicated zoom mechanic, the optical system is able to maintain consistent image quality throughout the zoom range. The distortion of the system changes from negative to positive as the focal length increases, with large positive distortion at 168 mm focal length. It is worth noting here that the field curvature does not change throughout the zoom range, the plot is showing a wider field of view, and the Petzval radius has more exaggerated departure from the image plane further from the optical axis.

The optical system was modified to be telecentric in image space by varying the position of the stop to maintain exit pupil location at infinity throughout the zoom range. The overall length of the system was increased significantly to maintain the stop position at the front focal plane. The same technique was used to optimize the system by having a merit function weighted to limit the angular magnification at the image plane. The modification to the system achieved the same 62, 82, and 168 mm focal lengths but required the field of view to be reduced from 30.4° down to 4° which reduced the speed of the lens to a F/7.9.

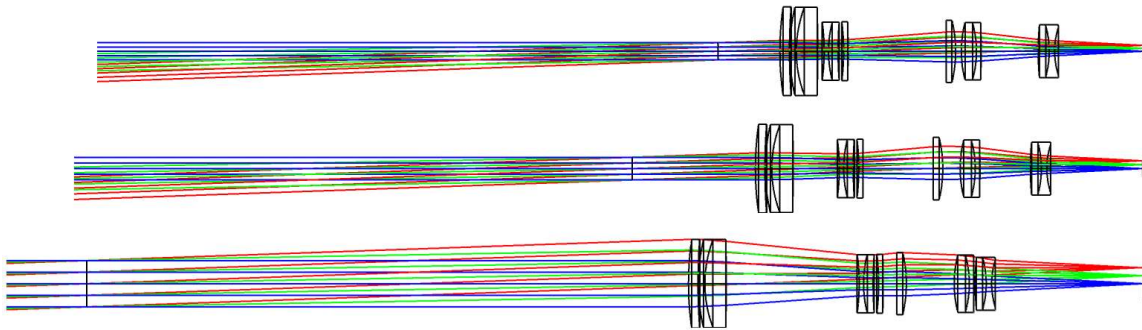


Figure 44: Zoom lens described in United States Patent 5,126,883. F7.9, 4° Field of View, with an effective focal length of 62 (top), 82 (middle), and 168 mm (bottom) with the stop positioned to maintain telecentricity.

Radius	Thickness (mm)	Refractive Index	Abbe No.
Infinity	d_1		
110.67	3.50	1.52	6.409
218.03	0.10		
69.14	2.40	1.81	2.540
44.75	7.80	1.52	6.409
-645.77	d_2		
-76.60	1.60	1.69	5.070
41.75	3.50	1.81	2.540
156.00	2.00		
-87.57	1.60	1.70	5.560
-695.19	d_3		
-840.52	3.43	1.61	5.850
-48.25	d_4	1.76	
42.00	5.50	1.66	5.700
-38.24	1.70	1.81	2.540
-343.79	d_5		
106.73	4.00	1.75	3.520
-35.00	2.00	1.71	5.390
28.12	55.66		

Table 8: Prescription for Study 2 which maintains telecentricity. F7.9, 4° Field of View, and an effective focal length of 62, 82, and 168 mm.

Variable	Config 1	Config 2	Config 3
d_1	22.60	45.00	220.00
d_2	2.38	16.88	48.59
d_3	35.91	25.68	5.10
d_4	2.11	6.37	17.51
d_5	20.89	18.47	0.47

Table 9: Addendum to the prescription for Study 2 showing the multi-configuration distances between lens groups.

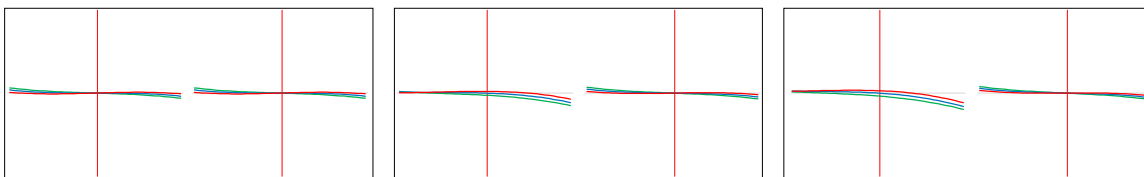


Figure 45: Tangential and Sagittal ray fan of Study 2, with a field of 1.4° at a focal length of 62, 82, and 168 mm, from left to right, using a scale of $\pm 200.0 \mu\text{m}$.

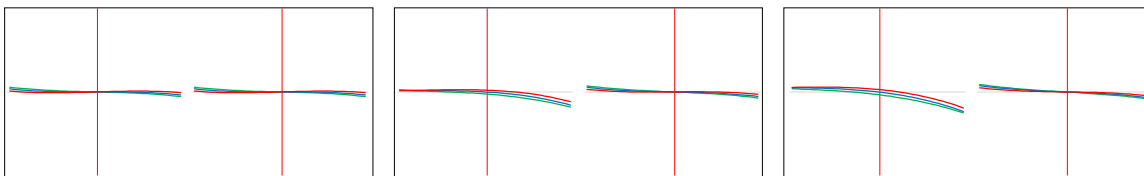


Figure 46: Tangential and Sagittal ray fan of Study 2, with a field of 1.4° at a focal length of 62, 82, and 168 mm, from left to right, using a scale of $\pm 200.0 \mu\text{m}$.

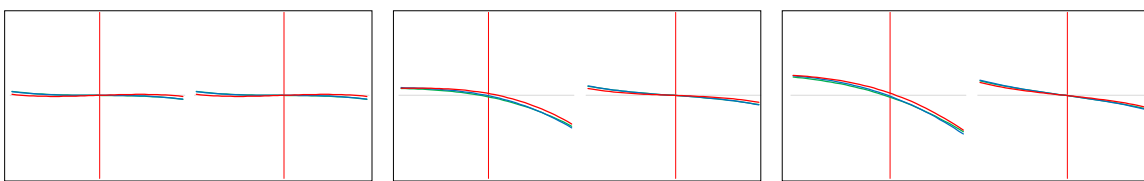


Figure 47: Tangential and Sagittal ray fan of Study 2, with a field of 2.0° at a focal length of 62, 82, and 168 mm, from left to right, using a scale of $\pm 200.0 \mu\text{m}$.

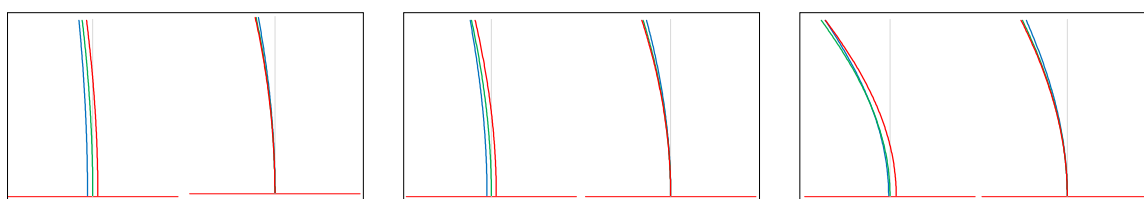


Figure 48: Field curvature and distortion plots of Study 2, at a focal length of 62, 82, and 168 mm from left to right, using a scale of $\pm 0.50 \text{ mm}$ and $\pm 1.0 \%$.

	W040	W131	W222	W220P	W311	W020	W111
62 mm	0.1599	0.4453	0.3592	0.0063	0.4174	-0.5111	-1.1524
82 mm	0.1546	0.6098	0.6891	0.011	0.8131	-0.4592	-1.191
168 mm	0.1997	1.3259	2.4134	0.0459	2.7836	-0.3687	-1.1056

Table 10: Seidel Coefficients for Study 2 showing the impact of each aberration on the system, at a focal length of 62, 82, and 168 mm from top to bottom, expressed in waves.

The image quality resulting from modifying the stop position was mostly unchanged with similar magnitude of aberrations, and remain consistent as the focal length increases. The distortion of the system is reduced to less than 1.0% across the field of view and remains negative in all configurations.

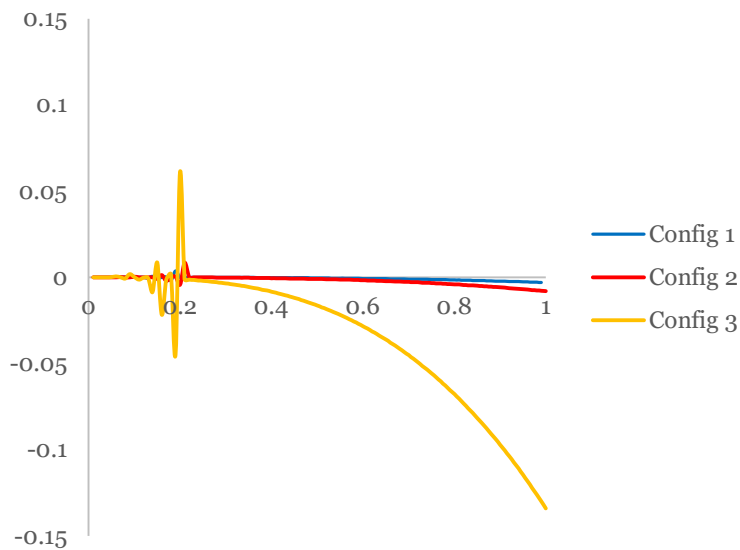


Figure 49: Visualization of the degree of telecentricity of the Study 2 expressed as a percentage change of the chief ray angle across a normalized pupil.

From this analysis, the degree of telecentricity of this study decreases as the focal length increases, being worst at a longer focal length at -0.14%. Additionally there is a perturbation for all three configurations near the origin.

5 Results and Discussion

The objective of this thesis was to study multi-configuration telecentric systems with an emphasis on achieving a generous depth of focus, maintaining low distortion, and controlling vignetting to provide a large useable field of view. The results of the thesis showed that zoom lenses with a telecentric stop position are capable of fulfilling the desired metrics, but not without compromise. The telecentric systems required a limited field of view and a much longer overall length.

The studies demonstrated a method for setting up and analyzing multi-configuration systems and optimizing the systems to maintain a telecentric stop position in different configurations. The image quality of the systems was evaluated, where the aberrations and field curvature were quantified and the system was corrected to minimize the contributions. In addition to image quality, the degree of telecentricity of the systems was analyzed to understand the change in chief ray slope throughout the zoom range. Further analysis can be done to assess the performance the telecentric qualities of the lens to assess the performance for applications where these qualities are essential.

Telecentric systems are characterized by their insensitivity to slight amounts of defocus. One method for visualizing the impact of defocus on an optical is to analyze the spot size through focus, where the system is imaged at positions before and after the ideal image plane. The size and shape of the spot indicates the magnitude and direction of blur in a defocused image. It can be expected that the spot size through focus will remain more consistent in a system were the ray bundle is tightly controlled and the chief ray maintains orthogonality to the image plane.

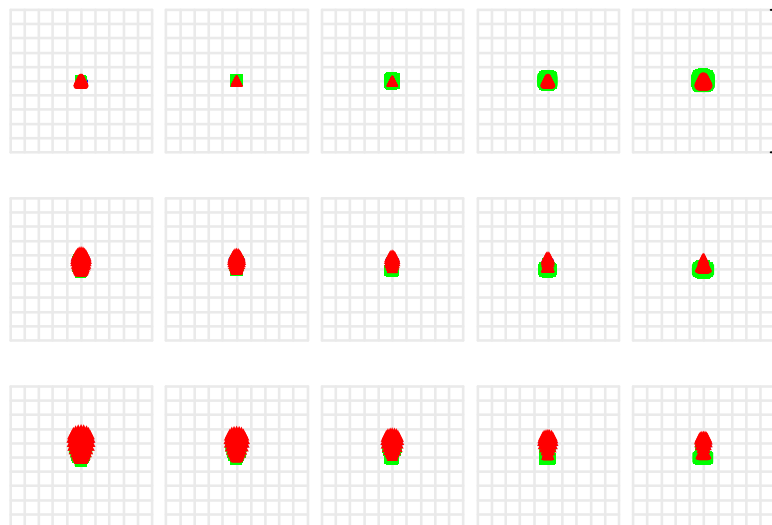


Figure 50: Through focus spot diagram of Study 1 at configuration 1 with field angle 0.0° (top), 1.4° (middle), and 2.0° (bottom) and the spot size at $-100\ \mu\text{m}$ through $+100\ \mu\text{m}$ (left to right) with a scale of $400\ \mu\text{m}$.

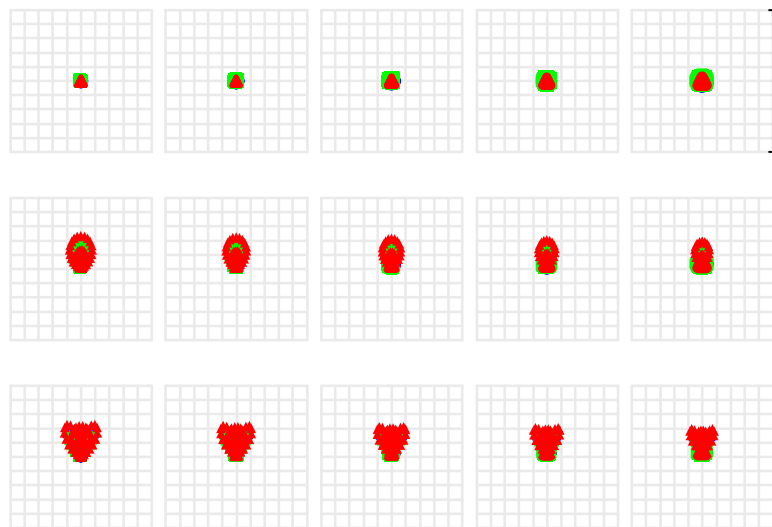


Figure 51: Through focus spot diagram of Study 1 at configuration 2 with field angle 0.0° (top), 1.4° (middle), and 2.0° (bottom) and the spot size at $-100\ \mu\text{m}$ through $+100\ \mu\text{m}$ (left to right) with a scale of $400\ \mu\text{m}$.

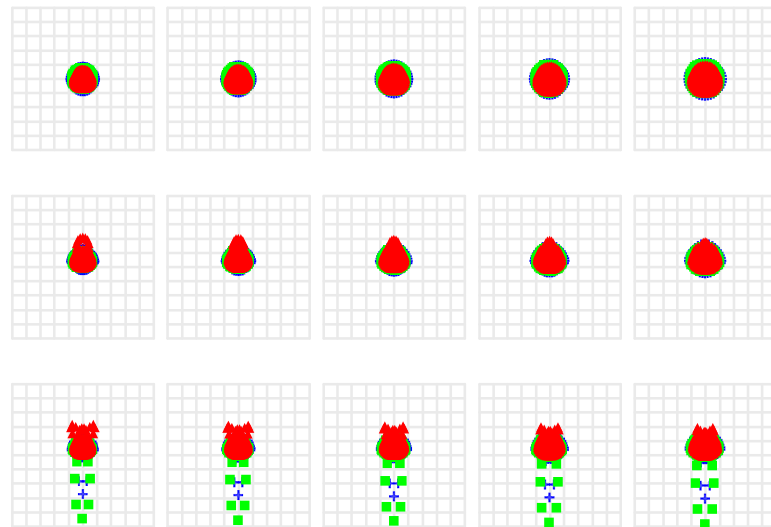


Figure 52: Through focus spot diagram of Study 1 at configuration 3 with field angle 0.0° (top), 1.4° (middle), and 2.0° (bottom) and the spot size at $-100 \mu\text{m}$ through $+100 \mu\text{m}$ (left to right) with a scale of $400 \mu\text{m}$.

It can be seen that the telecentric system from Study 1 has a spot size through focus which remains consistent along a $\pm 100 \mu\text{m}$ range. Where Configuration 1 shows the smallest spot sizes, it also experiences more change through focus than Configuration 2 or 3. For all configurations the spot size is larger at large field angles, and this is more exaggerated for the longer focal lengths, particularly at Configuration 3. However, the through focus spot size shows little change. These results are consistent with the degree of telecentricity results, showing Configuration 1 has the most variation in the chief ray slope.

A through focus spot diagram analysis was also performed on Study 2.

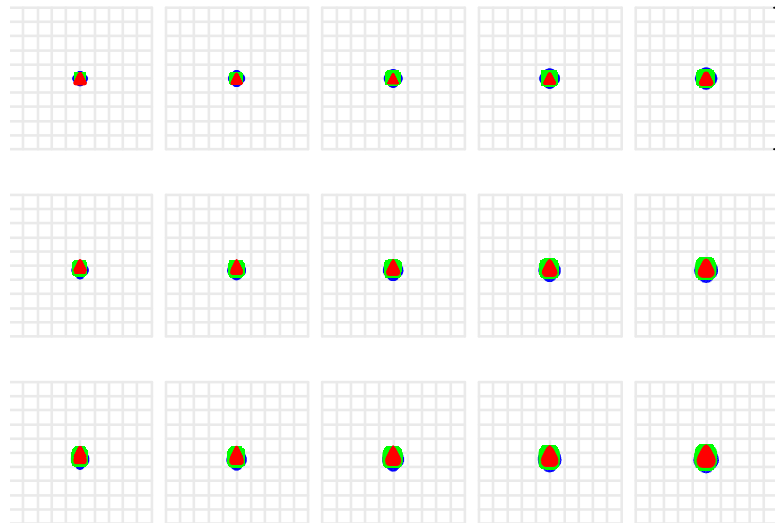


Figure 53: Through focus spot diagram of Study 2 at configuration 1 with field angle 0.0° (top), 1.4° (middle), and 2.0° (bottom) and the spot size at $-100 \mu\text{m}$ through $+100 \mu\text{m}$ (left to right) with a scale of $400 \mu\text{m}$.

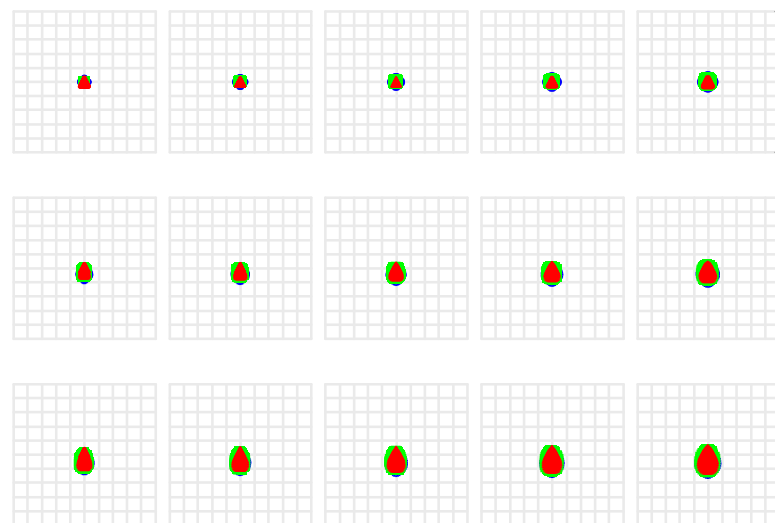


Figure 54: Through focus spot diagram of Study 2 at configuration 2 with field angle 0.0° (top), 1.4° (middle), and 2.0° (bottom) and the spot size at $-100 \mu\text{m}$ through $+100 \mu\text{m}$ (left to right) with a scale of $400 \mu\text{m}$.

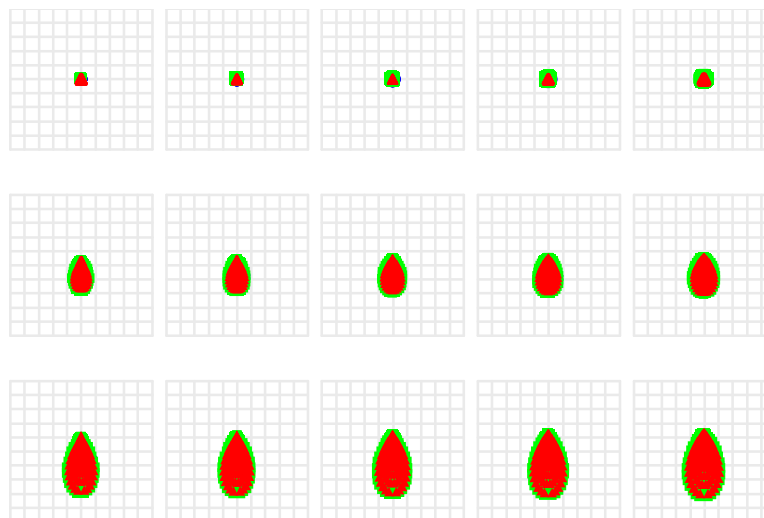


Figure 55: Through focus spot diagram of Study 2 at configuration 3 with field angle 0.0° (top), 1.4° (middle), and 2.0° (bottom) and the spot size at $-100\ \mu\text{m}$ through $+100\ \mu\text{m}$ (left to right) with a scale of $400\ \mu\text{m}$.

Study 2 also shows a consistent through focus spot diagram with the larger field angles having a larger spot, but the size and shape remains consistent. Configuration 3 is less consistent through focus than Configuration 1 and 2. Again, for all configurations the spot size is larger at large field angles, and this is more exaggerated for the longer focal lengths. However, the through focus remains very similar. Once again, these results are consistent with the degree of telecentricity results, showing Configuration 3 has the most variation in the chief ray slope.

Low distortion and orthogonality between object and image planes are also characteristics of telecentric systems. OpticStudio has a tool for evaluation of the grid distortion of a system which computes the coordinates of a grid of chief rays. The grid distortion plot shows a linear grid and marks the actual chief ray intercept for a ray. This can be used as a tool to visualize and quantify how closely to orthogonal the imaging systems performs.

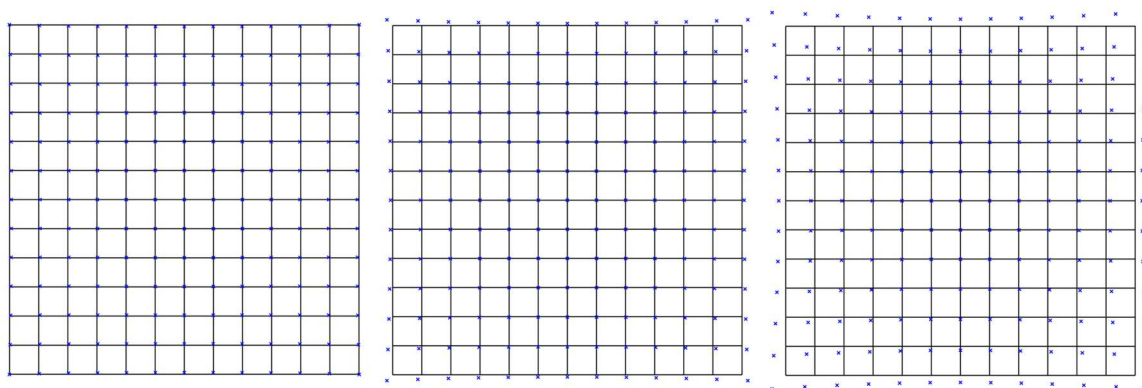


Figure 56: Grid Distortion plot of Study 1 at Configuration 1 (left), 2 (middle), and 3 (right) shown with an exaggerated 10x scale to clearly show distortion.

For Study 1, Configuration 1 has a maximum distortion of -0.0904% , Configuration 2 has a maximum distortion of 0.3315% , and Configuration 3 has a maximum distortion of 0.7783% . Although this is inconsistent with the results from the degree of telecentricity analysis, it is expected that the distortion would increase with a longer focal length.

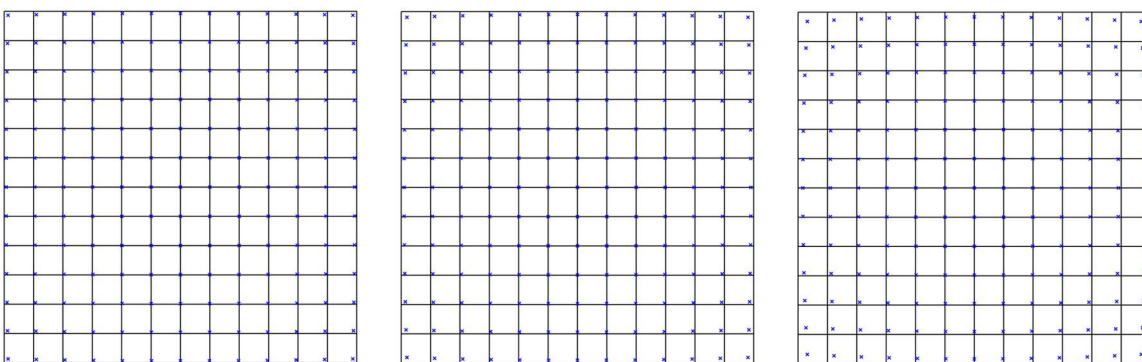


Figure 57: Grid Distortion plot of Study 2 at Configuration 1 (left), 2 (middle), and 3 (right) shown with an exaggerated 10x scale to clearly show distortion.

For Study 2, Configuration 1 has a maximum distortion of -0.2218% , Configuration 2 has a maximum distortion of -0.3235% , and Configuration 3 has a maximum distortion of -0.5260% . Again, it can be seen that the distortion increases with a longer focal length.

For both studies the field of view was limited to 4° to avoid vignetting in the system. Because the aperture stop is positioned at the front focal plane, for longer focal length systems the stop distance to the lens increases. This affects the overall length of the optical systems, resulting in a proportionately longer system than would be necessary for a non-telecentric system as well as only accommodating smaller field angles. This can be remedied by increasing the diameter of the lenses to accept larger input angles. This technique can be seen on many commercially available telecentric lenses with one or more lens groups having a much larger diameter than the other groups.

This thesis showed that the design of telecentric systems can accommodate multiple configurations with repeatable results. This was accomplished by modeling multi-configuration systems in a first-order approximation and verifying the simplified system could maintain telecentricity throughout different configurations. The third-order aberrations were numerically evaluated to understand the impact on the system and a method was determined for defining the degree of telecentricity of a system. Finally, through simulation, third-order optical systems were modeled to demonstrate the trade space of telecentric multi-configuration systems. Two optical systems were shown with a zoom ratio of 3, one with focal length of 25 to 75 mm, and a field of view of 4° with a maximum telecentricity of 0.2 %, and a second with a focal length of 62 to 168 mm, and a field of view of 4° with a maximum telecentricity of -0.14 %.

The method shown for developing a telecentric zoom lens provided a model with image quality comparable with similar non-telecentric systems. The trade space involves the physical dimensions of the optical system, the useable field of view, and degree of telecentricity. A method was developed to correctly identify the performance of a third-order system through the degree of telecentricity. Further work on the subject could evaluate the method demonstrated for object-sided telecentric systems, as well as investigating the first-order hypothesis of concatenation of two image-sided telecentric systems to achieve a double-sided telecentric system.

Appendix A - Glossary

Aberration function is a mathematical function used for characterizing waveform deformation by providing the optical path length at the exit pupil of a given ray as a function of the normalized field vector, \vec{H} , and the aperture vector, $\vec{\rho}$

Astigmatism aberration is a double plane symmetric aberration resulting from a meridian ray fan coming to focus at one point with a second orthogonal ray fan coming to focus at a different point

Coma aberration is a plane symmetric aberration, which is an off-axis aberration, where annual zones have different magnifications resulting a point that looks like a comet

Chromatic aberration is a condition which results in a change of optical power for a lens or system as a function of different wavelengths and can be either chromatic change of focus or chromatic change of magnification

Depth of field refers to the displacement of an object along the optical axis, where the image quality is maintained

Depth of focus refers to the displacement in image space along the optical axis, where the image quality is maintained

Distortion aberration is a plane symmetric aberration where the magnification of the optical system varies across the field of view

F-number is a metric used to describe the *speed* or relative aperture of a system and is the ratio of the focal length and the aperture diameter

Field curvature is an axially symmetric aberration of an optical system where there is a deviation from imaging to a plane such as a curved surface

Field of view is a metric used to describe the portion of the object that is included in the image

First-order approximation is a model an optical system using thin lenses assumes zero axial thickness of a lens, which allows the principal plan and thin lens to be coincident, it will also adopt the small angle approximation for rays near the optical axis.

Focal length is a metric used to describe the distance from the principal plane to the focal point

Lensmaker's equation is a tool to approximate the power of a lens as a function of the curvature and refractive index of the lens elements.

Marginal ray is the ray that passes through the edge of the aperture stop and through the center of the image

Numerical aperture is a metric used to describe the index of refraction and the sine of the half angle of the illumination cone, related to F-number

Optical power is a description of either a single lens (singlet) or an optical system containing multiple elements, to show the relationship between index of refraction, surface curvature and thickness to the focal length

Snell's law describes the relationship between the change in a ray slope at a boundary between two different media

Spherical aberration is an axially symmetric aberration and is the result of a difference between where the *marginal ray* and *chief ray* come to focus

Telephoto is an optical system or configuration which has a longer focal length and a field of view covering a narrow angle

Telecentric lenses are compound optical systems which maintain the centroid and height of objects relative to the image plane and are insensitive to slight defocus

Thin lens is a concept used to simplifying ray tracing by approximating a lens, the index thickness is assumed as 0 and the optical power results from the radius of curvature and index of refraction

Transverse ray aberration is a mathematical function for determining the magnitude of aberrations on a system by as a function of the distance between the paraxial ray and the real ray, orthogonally, along the optical axis

Vignetting is an obstruction of off-axis rays which are clipped by the aperture of a lens resulting in a reduction in illumination at the peripheral of the field of view.

Wide angle is an optical system or configuration which has a short focal length and a field of view covering a wide angle

Zoom lens is a multi-configuration optical system which adapts to accommodate many different environments. Typically these systems will be characterized by having a linear movement from a short focal length to a long focal length

Appendix B - Software Source Code

```

1 !This Zemax macro program plots the chief ray
2
3
4 !Written by Ross Terrill October 2020
5
6 !Modified from Wavefront Aberrations from Sasian.zpl
7 !Written by Jose Sasian, February 2013.
8
9 !Modified from illumination v1.zpl
10 !Written by Jose Sasian August 2016
11
12 !*****
13 !Defines variables and constants
14
15 DECLARE surf, double, 1, 104
16 DECLARE marg, double, 1, 104
17
18 wavel = 1
19
20 N=nsur()
21
22 pi2=3.1415926
23
24
25 RAYTRACE 0,0,0,1,wavel
26 yym=rayy(N)
27
28     w311=0
29     w040p=0
30
31 !*****
32 !Starts the iteration to calculate the coordinates
33
34 FOR k=3, N-1, 1
35 FOR j=1, 100, 1
36
37 RAYTRACE 0,0,0,j/100,wavel
38
39 rad=RADI(j)
40 if (rad==0)
41 rad=10e40
42 endif
43
44 njb=INDX(k-1)
45 nj=INDX(k)
46     index = INDX(k-1)
47     indexp = INDX(k)
48     IF isms(k-1) THEN njb = -njb
49     IF isms(k) THEN nj = -nj
50

```

```

51 !Trace marginal ray
52
53 RAYTRACE 0,0,0,j/100,wavel
54 ym=RAYY(k)
55 um=(RAYM(k)/RAYN(k))
56 umb=(RAYM(k-1)/RAYN(k-1))
57 im=umb+ym/rad
58 A=njb*im
59 alfa=ym/rad
60 del=um/nj-umb/njb
62 !Trace chief ray
63
64 RAYTRACE 0,j/100, 0, 0, wavel
65 yc=RAYY(k)
66 uc=(RAYM(k)/RAYN(k))
67 ucb=(RAYM(k-1)/RAYN(k-1))
68 ic=ucb+yc/rad
69 B=njb*ic
70 alfap=yc/rad
71 delp=uc/nj-ucb/njb
72
73 !Calculates the Lagrange invariant and checks its value
74
75 LG=nj*(uc*ym-yc*um)
76
77 w311=- (1/2)*(B*B*B*ym*(1/(nj*nj)-1/(njb*njb))-B*(LG+B*ym)*yc*(1/nj-1/njb)/rad)
78 w040p=(-1/8)*B*B*delp*yc
79
80 surf(j)=j
81 marg(j)=(4*w040p/(indexp*yc)-w311/(indexp*ym))+marg(j)
82
83 NEXT
84 NEXT
85
86 !*****
87
88 FOR j=1, 100, 1
89 marg(j) = marg(j)*100
90 Print marg(j)
91 NEXT
92
93 IF marg(100)>0
94 ymx = marg(100)
95 ymn = -1*ymx
96 ELSE
97 ymx = -1*marg(100)
98 ymn = -1*ymx
99 ENDIF
100
101 !Makes a plot of the Telecentricity
102 PLOT NEW
103 PLOT TITLE, "Degree of Telecentricity"
104 PLOT TITLEX, "X"
105 PLOT TITLEY, "Y"
106 PLOT FORMATX, "%2.1f"
107 PLOT FORMATY, "%1.3f"
108 PLOT RANGEX, 0, 100
109 PLOT RANGEY, ymn,ymx
110 PLOT DATA, surf, marg, j-1, 1, 0, 0
111 PLOT GO
112 !*****

```

References

- [1] Chang, Matthew, "Pupil aberration in modular zoom lens design," Ph.D. dissertation, College of Optical Sciences, University of Arizona, AZ, USA, 1998 [Online].
- [2] Miks, Novak, "Design of a double-sided telecentric zoom lens," Department of Physics, Czech Technical University, Prague, Czech Republic, 2012 [Online].
- [3] Hu, Haosheng "Tutorial of Telecentric Lens" College of Optical Sciences, University of Arizona, 2016 [Online]
- [4] Smith, Warren J. *Modern Optical Engineering Fourth Edition* (New York, NY, McGraw-Hill 2008)
- [5] Tomoyuki Matsuyama, Yasuhiro Ohmura, and David M. Williamson "The lithographic lens: its history and evolution", Proc. SPIE 6154, Optical Microlithography XIX, 615403, 2006 [Online].
- [6] Sasián, José. *Introduction to Aberrations in Optical Imaging Systems* (Cambridge, UK, Cambridge University Press, 2013)
- [7] Sasián, José. *Introduction to Lens Design* (Cambridge, UK, Cambridge University Press, 2019)